Limiting heavy-quark and gluonphilic real dark matter

Sukanta Dutta[*]
Delhi School of Analytics, Institution of Eminence, University of Delhi, Delhi 110007, India and SGTB Khalsa College, University of Delhi, Delhi 110007, India

Lalit Kumar Saini[†]
Department of Physics and Astrophysics, University of Delhi, Delhi 110007, India

(Received 2 February 2022; accepted 11 July 2022; published 27 July 2022)

We investigate the phenomenological viability of real spin half, zero, and one dark matter candidates, which interact predominantly with third-generation heavy quarks and gluons via the 28 gauge invariant higher-dimensional effective operators. The corresponding Wilson coefficients are constrained one at a time from the relic density $\Omega^{\rm DM}h^2 \approx 0.1198$. Their contributions to the thermally-averaged annihilation cross sections are shown to be consistent with the FermiLAT and H.E.S.S. experiments' projected upper bound on the annihilation cross section in the $b\bar{b}$ mode. The tree-level gluonphilic and one-loop induced heavy-quarkphilic dark matter (DM) nucleon direct detection cross sections are analyzed. The non-observation of any excess over expected background in the case of recoiled Xe nucleus events for spin-independent DM-nucleus scattering in XENON-1T sets the upper limits on the 18 Wilson coefficients. Our analysis validates the real DM candidates for the large range of accessible mass spectrum below 2 TeV for all but one interaction induced by the said operators.

DOI: 10.1103/PhysRevD.106.015026

I. INTRODUCTION

Regardless of the unequivocal astrophysical evidences from rotation velocity curves [1] via mass-to-luminosity ratio, Bullet Cluster [2], and precision measurements of the cosmic microwave background (CMB) from WMAP [3] and PLANCK [4] satellites etc., we have no clue about the fundamental nature of dark matter (DM) which forms the dominant matter component of the Universe. Dedicated experiments for the direct detection of DM such as LUX [5], XENON-1T [6], DarkSide50 [7], PandaX-4T [8] and CRESST-III [9], PICO-60 [10], and PICASSO [11] are designed to measure the momentum of the recoiled atom and/or nucleus due to the scattering of DM particles off the subatomic constituents of the detector material [12–14]. We have not seen any significant signal excess over the expected background yet. PandaX-4T [8] and PICO-60 [10] have recently lowered the upper limits of the measured sensitivities at 90% C.L. corresponding to (a) spin-independent cross sections at 3.3×10^{-47} cm^2 for 30 GeV DM and (b) spin-dependent cross sections at 2.5×10^{-41} cm^2 for 25 GeV DM, respectively. There are efforts being made to understand the nature of DM interactions by indirectly detecting DM resulting from DM pair annihilations to SM particles using space-based facilities such as Fermi-LAT [15], PLANCK data [4], MAGIC [16], and some ground-based large neutrino detectors such as HESS [17], Ice Cube [18], ANTARES [19], Super-Kamiokande [20], etc.

Several experiments, past and ongoing, have constrained a plethora of viable UV complete dark matter models formulated by writing renormalizable Lagrangians with heavy non-SM mediators (spin $0^{\pm}$, $1/2$, 1, 2) facilitating interactions between DM and SM particles [21–31]. The models with Higgs bosons as mediators have been excluded by the recent collider experiments [32]. Analogous analysis has also been performed in the domain of the effective field theory (EFT) for the EW-Boson-philic DM operators [33–35]. Recently, the GAMBIT Collaboration performed a global analysis for signatures of SM gauge singlet Dirac fermion DM at LHC in the EFT setup with simultaneous activation of 14 effective operators constructed in association with light quarks, gluons, and photons (up to mass dimension seven) where the authors have disfavored the exclusive contribution of DM $\leq$ 100 GeV [36]. The possibility of sterile neutrinos as DM candidates interacting with the third-generation fermions has been recently analyzed in the EFT approach in Ref. [37]. The collider signatures of the effective leptophilic DM operators have been studied for the proposed ILC

[*]Sukanta.Dutta@gmail.com
[†]sainikrlalit@gmail.com

through $e^+e^- \to \gamma + \not{E}_T$ [38–44] and $e^+e^- \to Z^0 + \not{E}_T$ [45,46] channels. Sensitivity analysis for DM-quark effective interactions at LHC have been performed [47–51] in a model-independent way for the dominant (a) monojet + $\not{E}_T$, (b) mono-b jet + $\not{E}_T$, and (c) mono-t jet + $\not{E}_T$ processes.

Various topphilic DM inspired models have been studied and constrained [52–58] by the cosmological relic density criteria, direct detection and indirect detection experiments. The interactions of heavy-quarkphilic DM are also constrained by the ongoing collider experiments. The CMS [59,60] and ATLAS [61] Collaborations investigated the dominant scalar-mediated production of t-quarkphilic DM particles in association with a single top quark or a pair of $t\bar{t}$. The CMS Collaboration recently conducted an exclusive search analysis for the b-philic DM in reference [62]. Many authors in the literature have explored monojet + $\not{E}_T$ mode at the LHC for the viable signatures of the scalar current induced heavy-quarkphilic DM interactions [51,63–65]. A comprehensive search analysis for heavy scalar mediated topphilic DM models for monojets+ $\not{E}_T$, mono-Z, mono-h, and $t\bar{t}$ pair productions at LHC can be found in [66,67].

The phenomenology of spin 1/2, 0, and 1 real DM deserves a special mention in the context of their contributions to the DM-nucleon scattering events in the direct detection experiments. In the absence of the contributions from vanishing vector operators for Majorana and real vector DM, the spin-independent DM-nucleon scattering cross sections are found to be dominated by the respective scalar and dimension-8 twist operators [68–75]. The pseudoscalar current contribution to the DM-nucleon scattering cross section is found to be spin dependent and velocity suppressed. Similar studies have also been undertaken for leptophilic real DM candidates [39,40].

In this context, it is worthwhile to investigate the WIMP DM phenomenology induced by heavy-quarkphilic and gluonphilic scalar, pseudoscalar, axial-vector, and twist-2 real-DM operators and explore whether they satisfy the relic density criteria and other experimental constraints for a DM mass between 10 GeV and 2 TeV. We introduce the effective Lagrangian for real spin 1/2, 0, and 1 DM particles in Sec. II. In Sec. III, we discuss the phenomenology of the dark matter. We investigate the cosmological constraints on the DM in Sec. III A. In Sec. III B, we predict and analyze the thermally-averaged DM pair-annihilation cross section. Section III C details the computation of DM-nucleon scattering cross sections and expected recoil nucleus event(s) for XENON-1T [6] setup. Section IV summarizes our study and observations.

II. HEAVY-QUARK AND GLUONPHILIC DM EFFECTIVE OPERATORS

It is a fact that in a beyond the standard model (BSM) renormalizable gauge theory, as long as the energy range of DM-SM interaction is much below the mediator mass, the study of DM interactions can be restricted by the DM and SM degrees of freedom and their symmetries.

The higher-dimensional effective operators are obtained from the BSM Lagrangian by writing the operator product expansion of currents in the limit $p^2/m^2_{\rm Med.} \ll 1$, where p^μ represents the four-momentum of the virtual mediator of mass $m_{\rm Med}$. This facilitates the effective contact interaction between DM and any SM third-generation heavy quark/gluon, assuming that the mediator mass scale $m_{\rm Med}$. is of the order of the effective theory cutoff ($\sim\Lambda_{\rm eff}$), which is much heavier than the masses of the SM and DM fields in general.

For example, in renormalizable models, the interaction between a Majorana DM χ and a third-generation quark ψ can be written as

$$\mathcal{L}^{\rm Dim.\,4} = \bar{\psi}(a + b\gamma_5)\chi\eta + \bar{\psi}\gamma^\mu(c + d\gamma_5)\chi\zeta_\mu + {\rm H.c.} \qquad (1)$$

where η and ζ_μ are electrically charged scalar and vector fields, respectively. This interaction Lagrangian facilitates the Majorana DM-quark interaction via t-channel exchange of the heavy η and/or ζ_μ. Thus, expanding the propagator in powers of $p^2/m^2_{\rm Med}$, yields the higher-dimensional effective four-fermion interaction for Majorana DM and heavy quarks. The scalar, pseudoscalar, axial-vector, and twist-2 operators are all induced by this expansion [68]. When compared to a spin-2 graviton mediated model, the twist operator corresponds to the contribution from traceless part of the energy-momentum tensor $T^{\mu\nu}$ [76]. In various WIMP-inspired renormalizable electroweak models, such effective interactions between the SM and Majorana DM particles are also realized by s-channel processes, where the interactions are mediated by non-SM heavy scalar/pseudoscalar/axial-vector or spin-2 tensor particles [77,78].

Since the DM-gluon interactions can be naturally realized via one-loop interactions of the DM particles either with SM heavy quarks or BSM nonsinglet colored spin 1/2, 0, and 1 exotics at the next order in the strong coupling constant, it becomes all the more necessary to include the study of effective operators constructed independently with a Majorana DM bilinear and a pair of gluons at the leading order of $\sim\alpha_s/\pi$.

The phenomenological effective Lagrangian for the heavy-quarkphilic and gluonphilic Majorana DM, χ, is written as

$$\mathcal{L}^\chi_{\rm eff} = \frac{C^q_{\chi_S}}{\Lambda^3}\mathcal{O}^q_{\chi_S} + \frac{C^q_{\chi_{\rm PS}}}{\Lambda^3}\mathcal{O}^q_{\chi_{\rm PS}} + \frac{C^g_{\chi_S}}{\Lambda^4}\mathcal{O}^g_{\chi_S} + \frac{C^g_{\chi_{\rm PS}}}{\Lambda^4}\mathcal{O}^g_{\chi_{\rm PS}} + \frac{C^q_{\chi_{\rm AV}}}{\Lambda^2}\mathcal{O}^q_{\chi_{\rm AV}} + \frac{C^p_{\chi_{T_1}}}{\Lambda^4}\mathcal{O}^p_{\chi_{T_1}} + \frac{C^p_{\chi_{T_2}}}{\Lambda^5}\mathcal{O}^p_{\chi_{T_2}}. \qquad (2)$$

The $\mathcal{O}^q_{\chi_S}, \mathcal{O}^q_{\chi_{\rm PS}}, \mathcal{O}^q_{\chi_{\rm AV}}$, and $\mathcal{O}^q_{\chi_{T_i}}$ representing the third-generation quarkphilic scalar, pseudoscalar, axial-vector and twist-2 type-1 and type 2 operators, respectively along with $\mathcal{O}^g_{\chi_S}, \mathcal{O}^g_{\chi_{\rm PS}}$, and $\mathcal{O}^g_{\chi_{T_i}}$ representing the gluonphilic scalar, pseudoscalar, and twist-2 type-1 and type-2 operators, respectively are defined as

$$\begin{aligned}
&\mathcal{O}^q_{\chi_S} = m_q(\bar{\chi}\chi)(\bar{q}q); && \mathcal{O}^g_{\chi_S} = \frac{\alpha_s}{\pi} m_\chi(\bar{\chi}\chi)G^A_{\mu\nu}G^{A\mu\nu};\\
&\mathcal{O}^q_{\chi_{\rm PS}} = m_q(\bar{\chi}\gamma_5\chi)(\bar{q}\gamma_5 q); && \mathcal{O}^g_{\chi_{\rm PS}} = \frac{\alpha_s}{\pi} m_\chi(i\bar{\chi}\gamma_5\chi)G^A_{\mu\nu}\widetilde{G^{A\mu\nu}};\\
&\mathcal{O}^q_{\chi_{\rm AV}} = (\bar{\chi}\gamma_\mu\gamma_5\chi)(\bar{q}\gamma^\mu\gamma_5 q); &&\\
&\mathcal{O}^q_{\chi_{T_1}} = (\bar{\chi}i\partial^\mu\gamma^\nu\chi)\mathcal{O}^q_{\mu\nu}; && \mathcal{O}^g_{\chi_{T_1}} = (\bar{\chi}i\partial^\mu\gamma^\nu\chi)\mathcal{O}^g_{\mu\nu};\\
&\mathcal{O}^q_{\chi_{T_2}} = (\bar{\chi}i\partial^\mu i\partial^\nu\chi)\mathcal{O}^q_{\mu\nu}; && \mathcal{O}^g_{\chi_{T_2}} = (\bar{\chi}i\partial^\mu i\partial^\nu\chi)\mathcal{O}^g_{\mu\nu}.
\end{aligned} \tag{3}$$

The second rank twist-tensor currents $\mathcal{O}^q_{\mu\nu}$ and $\mathcal{O}^g_{\mu\nu}$ for the heavy quarks and gluons respectively are given as

$$\begin{aligned}
\mathcal{O}^q_{\mu\nu} \equiv\ & i\frac{1}{2}\overline{q_L}\left(D_{\mu L}\gamma_\nu + D_{\nu L}\gamma_\mu - \frac{1}{2}g_{\mu\nu}\not{D}_L\right)q_L\\
&+ i\frac{1}{2}\overline{q_R}\left(D_{\mu R}\gamma_\nu + D_{\nu R}\gamma_\mu - \frac{1}{2}g_{\mu\nu}\not{D}_R\right)q_R
\end{aligned} \tag{4a}$$

$$\mathcal{O}^g_{\mu\nu} \equiv \left[(G^A)_\mu{}^\rho (G^A)_{\nu\rho} - \frac{1}{4}g_{\mu\nu}(G^A)_{\rho\sigma}(G^A)^{\rho\sigma}\right], \tag{4b}$$

where D_{μ_L} and D_{μ_R} are the covariant derivatives for left- and right-handed quarks respectively in SM. The contribution from the vector operator vanishes for the real particles. We exclude the contribution of the dimension-9 twist-2 type-2 operators $\mathcal{O}^g_{\chi_{T_2}}$ in our analysis because we are only interested in the effective operators up to mass dimension-8.

We extend the domain of our analysis to include the effective contact interactions of real scalar ϕ^0 and vector V^0_μ DM candidates with SM third-generation heavy quarks and gluons. The effective scalar DM Lagrangian are given as

$$\mathcal{L}^{\phi^0}_{\rm eff} = \frac{C^q_{\phi^0_S}}{\Lambda^2}\mathcal{O}^q_{\phi^0_S} + \frac{C^g_{\phi^0_S}}{\Lambda^2}\mathcal{O}^g_{\phi^0_S} + \frac{C^p_{\phi^0_{T_2}}}{\Lambda^4}\mathcal{O}^p_{\phi^0_{T_2}}, \tag{5}$$

where

$$\begin{aligned}
&\mathcal{O}^q_{\phi^0_S} = (\phi^0\phi^0)m_q(\bar{q}q); && \mathcal{O}^g_{\phi^0_S} = \frac{\alpha_s}{\pi}(\phi^0\phi^0)G^A_{\mu\nu}G^{A\mu\nu};\\
&\mathcal{O}^q_{\phi^0_{T_2}} = (\phi^0 i\partial^\mu i\partial^\nu\phi^0)\mathcal{O}^q_{\mu\nu}; && \mathcal{O}^g_{\phi^0_{T_2}} = (\phi^0 i\partial^\mu i\partial^\nu\phi^0)\mathcal{O}^g_{\mu\nu}.
\end{aligned} \tag{6}$$

The $\mathcal{O}^{q/g}_{\phi^0_S}$ and $\mathcal{O}^{q/g}_{\phi^0_{T_2}}$ are the scalar and second rank twist-2 type-2 operators respectively. There are no contributions from pseudoscalar and axial vector currents for the scalar DM operators.

The effective vector DM Lagrangian is given as

$$\begin{aligned}
\mathcal{L}^{V^0}_{\rm eff} =\ & \frac{C^q_{V^0_S}}{\Lambda^2}\mathcal{O}^q_{V^0_S} + \frac{C^q_{V^0_{\rm PS}}}{\Lambda^4}\mathcal{O}^q_{V^0_{\rm PS}} + \frac{C^g_{V^0_S}}{\Lambda^2}\mathcal{O}^g_{V^0_S} + \frac{C^g_{V^0_{\rm PS}}}{\Lambda^4}\mathcal{O}^g_{V^0_{\rm PS}}\\
&+ \frac{C^q_{V^0_{\rm AV}}}{\Lambda^2}\mathcal{O}^q_{V^0_{\rm AV}} + \frac{C^p_{V^0_{T_2}}}{\Lambda^4}\mathcal{O}^p_{V^0_{T_2}}.
\end{aligned} \tag{7}$$

The heavy quarkphilic $\mathcal{O}^q_{V^0_S}$, $\mathcal{O}^q_{V^0_{\rm PS}}$, $\mathcal{O}^q_{V^0_{\rm AV}}$, $\mathcal{O}^q_{V^0_{T_2}}$ representing the third-generation quarkphilic scalar, pseudoscalar, axial-vector and twist-2 type-2 operators respectively and gluonphilic $\mathcal{O}^g_{V^0_S}$, $\mathcal{O}^g_{V^0_{\rm PS}}$, and $\mathcal{O}^g_{V^0_{T_2}}$ operators corresponding to the scalar, pseudoscalar and second rank twist-2 type-2 interactions, respectively are defined as

$$\begin{aligned}
\mathcal{O}^q_{V^0_S} &= (V^0)^\rho (V^0)_\rho m_q(\bar{q}q);\\
\mathcal{O}^g_{V^0_S} &= \frac{\alpha_s}{\pi}(V^0)^\rho (V^0)_\rho G^A_{\mu\nu}G^{A\mu\nu};\\
\mathcal{O}^q_{V^0_{\rm PS}} &= (V^0)^{\rho\sigma}\widetilde{(V^0)}_{\rho\sigma} m_q(i\bar{q}\gamma_5 q);\\
\mathcal{O}^g_{V^0_{\rm PS}} &= \frac{\alpha_s}{\pi}(V^0)^{\rho\sigma}\widetilde{(V^0)}_{\rho\sigma} G^A_{\mu\nu}\widetilde{G^{A\mu\nu}};\\
\mathcal{O}^q_{V^0_{\rm AV}} &= i\epsilon_{\mu\nu\rho\sigma}(V^0)^\mu i\partial^\nu (V^0)^\rho \bar{q}\gamma^\sigma\gamma_5 q;\\
\mathcal{O}^q_{V^0_{T_2}} &= (V^\rho)i\partial^\mu i\partial^\nu (V_\rho)\mathcal{O}^q_{\mu\nu};\\
\mathcal{O}^g_{V^0_{T_2}} &= (V^\rho)i\partial^\mu i\partial^\nu (V_\rho)\mathcal{O}^g_{\mu\nu},
\end{aligned} \tag{8}$$

where $\epsilon^{\mu\nu\rho\sigma}$ is the totally antisymmetric tensor with $\epsilon^{0123} = +1$.

In this study, each operator's phenomenology is investigated independently, assuming that the unique interaction contributes to the total relic density for DM.

III. PHENOMENOLOGICAL CONSTRAINTS ON REAL DM

A. Contribution of DM to the relic density

The present day relic abundance of the DM species $n_{\rm DM}(t)$ can be calculated by solving the Boltzmann equation

$$\frac{dn_{\rm DM}}{dt} + 3H_0 n_{\rm DM} = -\langle\sigma_{\rm ann}|\vec{v}_{\rm DM}|\rangle((n_{\rm DM})^2 - (n^{\rm eq}_{\rm DM})^2), \tag{9}$$

where $n^{\rm eq}_{\rm DM}$ is the DM number density at thermal equilibrium, H_0 is the Hubble constant, $|\vec{v}_{\rm DM}|$ is relative velocity of the DM pair and $\langle\sigma_{\rm ann}|\vec{v}_{\rm DM}|\rangle$ is the thermal average of the annihilation cross section [79]. It is customary to parametrize $\rho_{\rm DM} \equiv \Omega_{\rm DM}h^2\rho_c$, where $\rho_c \equiv 1.05373 \times 10^{-5}h^2/c^2$ GeV cm^{-3} is the critical density of the Universe and dimensionless h is the current Hubble constant in units of 100 km/s/Mpc. Solving the Boltzmann equation [80] we then get

$$\Omega^{\mathrm{DM}} h^2 = \frac{\rho^{\mathrm{DM}}}{\rho_{\mathrm{critical}}} h^2 \approx 0.12 \left(\frac{2.2 \times 10^{-26}\ \mathrm{cm}^3/\mathrm{s}}{\langle \sigma_{\mathrm{ann}} |\vec{v}_{\mathrm{DM}}| \rangle} \right) \left(\frac{80}{g_{\mathrm{eff}}} \right)^{1/2} \left(\frac{m_{\mathrm{DM}}/T_F}{23} \right), \tag{10}$$

where parameter $x_F \equiv m_{\mathrm{DM}}/T_F$ is a function of degrees of freedom of the DM g, the effective massless degrees of freedom g_{eff} ($\sim$106.75 and 86.75 above m_t and m_b mass thresholds, respectively) at freeze-out temperature T_F,

$$x_F = \ln \left[a(a+2) \sqrt{\frac{45}{8}} \frac{g M_{\mathrm{pl}}}{2\pi^3} \frac{m_{\mathrm{DM}} \langle \sigma_{\mathrm{ann}} |\vec{v}_{\mathrm{DM}}| \rangle}{\sqrt{x_F} g_{\mathrm{eff}}(x_F)} \right]; \quad a \sim \mathcal{O}(1) \quad \text{and} \quad M_{\mathrm{pl}} = 1.22 \times 10^{19}\ \mathrm{GeV}. \tag{11}$$

The predicted DM relic density $\Omega^{\mathrm{DM}} h^2$ of 0.1138 ± 0.0045 and 0.1198 ± 0.0012 by the WMAP [3] and Planck [4] Collaborations, respectively restrict the thermal averaged DM annihilation cross section $\langle \sigma |\vec{v}_{\mathrm{DM}}| \rangle \geq 2.2 \times 10^{-26}\ \mathrm{cm}^3\ \mathrm{s}^{-1}$ as a smaller thermally-averaged cross section would render a large DM abundance which will overclose the Universe. We have analytically calculated the DM pair-annihilation cross sections to a pair of third-generation heavy quarks and gluons in Appendix A.

We investigate the DM relic density contributions propelled by the thermally-averaged annihilation cross sections given in Appendix B corresponding to the scalar, pseudoscalar, axial-vector and twist-2 currents of the heavy quarks for a given Majorana/scalar/vector DM. The annihilation channels induced by the scalar, pseudoscalar, and twist-2 currents of gluons also contribute to the relic abundance of Majorana, scalar and vector DM.

Throughout our investigation, we assumed that the operators would be actuated one at a time. As a result, the constraints on all 28 Wilson coefficients $|C^{q,g}_{\mathrm{DM}_i O_j}/\Lambda^n|$ in TeV^{-n} ($\mathrm{DM}_i \equiv \chi, \phi^0, V^0$, and $O_j \equiv S/\mathrm{PS}/\mathrm{AV}/T_1/T_2$ are derived by triggering the lone contribution from the associated operator to fulfill the relic density $\Omega^{\mathrm{DM}} h^2 \approx 0.1198 \pm 0.0012$ [4]. Due to its only action, these constraints can be regarded as a cosmologically acceptable lower limits on the corresponding Wilson coefficients, which translate to upper bounds on the respective cutoffs $|C^{q,g}_{\mathrm{DM}_i O_j}|^{-1/n} \Lambda$ in units of TeV for a given DM mass. When the Wilson coefficient is greater than its lower limit for a given DM mass, it partially meets the relic density.

It is important to note that because we can raise the annihilation cross section by turning on more Wilson coefficients, we can easily imagine a scenario in which they all reside below their lower limit without overclosing the Universe with DM. To put it another way, if we set two distinct Wilson coefficients to their lower limits for a given DM mass, we plainly underproduce DM because the overall annihilation cross section is larger. Therefore, in order to be consistent with a multiple species of DM model satisfying the relic density constraint, this lower bound on the specific Wilson coefficient will further reduce when more than one coupling are triggered simultaneously. However, the rest of our analysis is focused on the scenario where the sole operator contributes to the relic density.

For numerical computation of the DM relic density, we have used MadDM [81,82], which implements the exact and closed expression for thermally-averaged annihilation cross section as discussed by the authors in Ref. [79]. The input model file required by the MadDM is generated using FeynRules [83,84], which calculates all the required couplings and Feynman rules by using the full Lagrangian given in Eqs. (3), (6), and (8) corresponding to Majorana, scalar and vector DM particles, respectively. We have further verified and validated our numerical results from micrOMEGAs [85]. The constant relic density contours are depicted in Figs. 1–3 corresponding to Majorana, real scalar and real vector DM candidates respectively in the plane defined by $m_{\mathrm{DM}_i} - |C^{q,g}_{\mathrm{DM}_i O_j}|^{-1/n} \Lambda$.

The thermally-averaged DM pair-annihilation cross section is found to be $\sim 2 \times 10^{-26}\ \mathrm{cm}^3\ \mathrm{s}^{-1}$ corresponding to a relic density of 0.1198, which essentially provides the functional dependence and shape profile of the Wilson coefficients with the varying DM mass corresponding to each four-point effective operator. In order to understand the shape profile of the relic density contours, $\langle \sigma v \rangle$ may be expanded analytically in power series of $|v_{\mathrm{DM}}|^2$ and then the contribution of the leading terms may be investigated. The velocity of the DM at freeze-out is considered to be $0.3c$. We observe that

(a) Due to the constrained thermally-averaged cross section, the cutoff Λ for Majorana DM scalar and pseudoscalar operators in Figs. 1(a) and 1(b) varies as $(m_f m_\chi)^{1/3}$ and therefore shows a steep rise for topphilic DM in comparison to the bottomphilic case. However, the pseudoscalar contribution dominates over its scalar counterpart due to its contribution from the leading velocity-independent term in Eq. (B1b). The cutoffs for leading contributions from the quark-philic twist operator and velocity suppressed gluon-philic scalar, pseudoscalar, and twist operators are found to increase monotonously with increasing DM mass as $m_\chi^{3/4}$.

(b) The s-wave contribution in the thermal averaged annihilation cross section $\langle \sigma_{\mathrm{AV}} |\vec{v}_\chi| \rangle$ given in Eq. (B1c) is proportional to m_f^2 which follows from the chirality-conserving property of axial-vector operator [86]. The variation of $\langle \sigma_{\mathrm{AV}} |\vec{v}_\chi| \rangle$ with the increasing DM mass is found to be largely determined by the terms proportional to m_χ^2 in the converging power series expansion as explicitly shown in Eq. (B1c). As a consequence, to satisfy the relic density constraint, the cutoff varies with respect to DM mass as $(m_\chi |\vec{v}_\chi|)^{1/2}$, i.e., faster

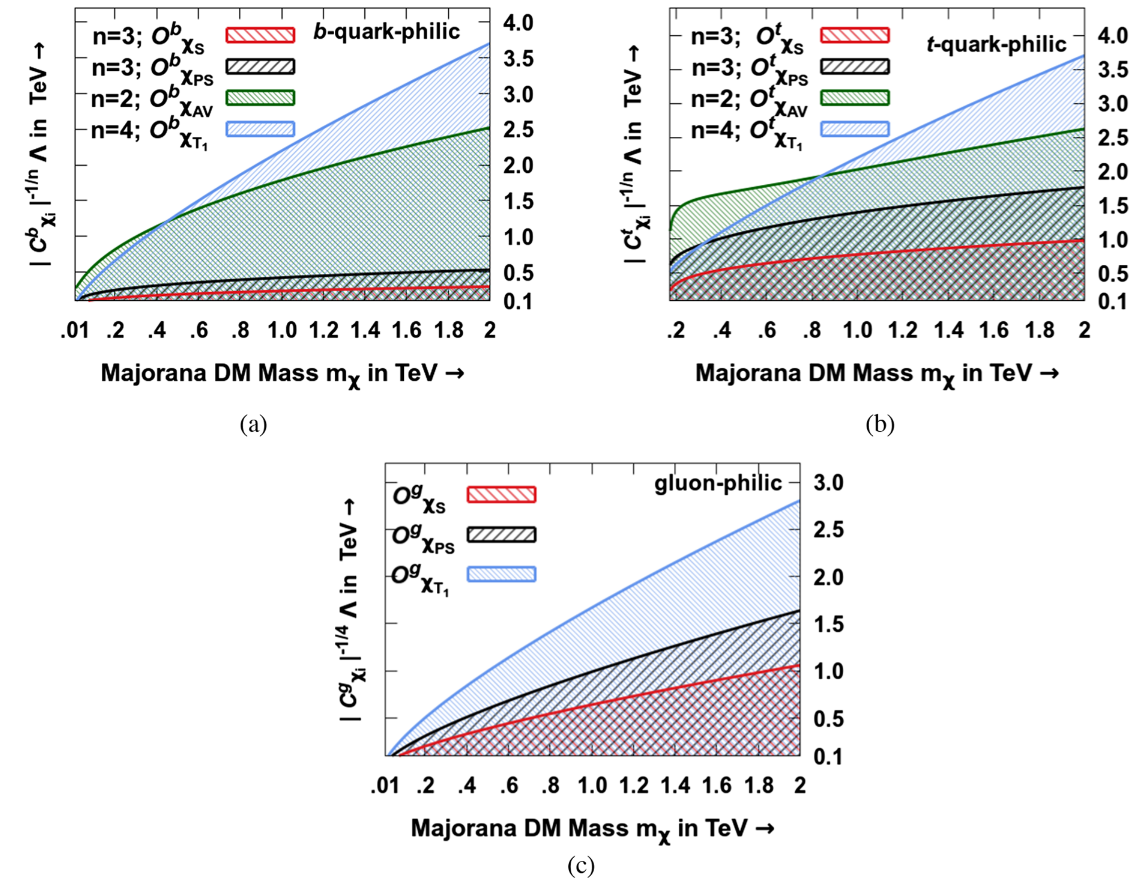

FIG. 1. We depict relic density contours satisfying $\Omega^\chi h^2 = 0.1198$ [4] and shaded cosmologically allowed regions in the plane defined by Majorana DM mass m_χ and $|C^{q/g}_{\chi_{S,PS,AV,T_1}}|^{-1/n}\Lambda$. The b-quarkphilic and t-quarkphilic Majorana DM contours in Figs. 1(a) and 1(b) are drawn corresponding to scalar, pseudoscalar, axial-vector and twist-2 type-1 operators. The gluonphilic Majorana DM contours in Fig. 1(c) are drawn for scalar, pseudoscalar, and twist-2 type-1 operators.

than scalar and pseudoscalar but slower than the twist operator, as shown in Figs. 1(a) and 1(b).

(c) The cutoffs for the scalar and twist operators induced by heavy-quarkphilic scalar and vector DM candidates are depicted in Figs. 2(a), 2(b), and 3(a), 3(b), respectively. In case of scalar interactions, the cutoffs are found to be independent of the DM masses, whereas the cutoff for the heavy-quarkphilic vector DM pseudoscalar operator is found to be monotonously increasing as $(m_{V^0})^{1/2}$. In case of twist operators, the cutoff variation goes as $(m_{\phi^0})^{1/2}$ for scalar DM, while for vector DM scenario, it is d-wave suppressed and goes as $|\vec{v}_{V^0}|^{1/2}(m_{V^0})^{3/4}$.

(d) the gluonphilic scalar, pseudoscalar, and twist interactions corresponding to Majorana DM are p-wave suppressed and the cutoff dependences are depicted in Fig. 1(c). The cutoffs corresponding to gluonphilic scalar, pseudoscalar, and twist operators for vector DM candidates are constrained to vary as $(m_{V^0})^{1/2}$, $|\vec{v}_{V^0}|^{1/4}(m_{V^0})^{3/4}$, and $|\vec{v}_{V^0}|^{1/2}(m_{V^0})^{3/4}$, respectively, as shown in Fig. 3(c). The observed relative suppression of the constrained cutoff for the twist operator is due to the velocity dependence. The same follows for the scalar DM candidates corresponding to the gluonphilic scalar and twist operators in Fig. 2(c).

B. Indirect detection of DM pairs

Today, the WIMP dark matter in the Universe is expected to be trapped in large gravitational potential wells, which further enhances the number density of DM in the region, resulting in frequent collisions among themselves. This facilitates DM-DM pair annihilation into a pair of SM particles (photons, leptons, hadronic jets, etc.) at the galactic center, in dwarf spheroidal galaxies (dSphs), galaxy clusters, and galactic halos. The dwarf spheroidal satellite galaxies of the Milky Way are especially promising targets for DM indirect detection due to their large dark matter content, low diffuse galactic γ-ray foregrounds as they travel the galactic distance, and lack of conventional astrophysical γ-ray production mechanisms. Their flux is observed by the satellite-based γ-ray observatory Fermi-LAT [87], PLANCK [4], primary cosmic rays measurements by AMS-02 [88,89] on the International Space

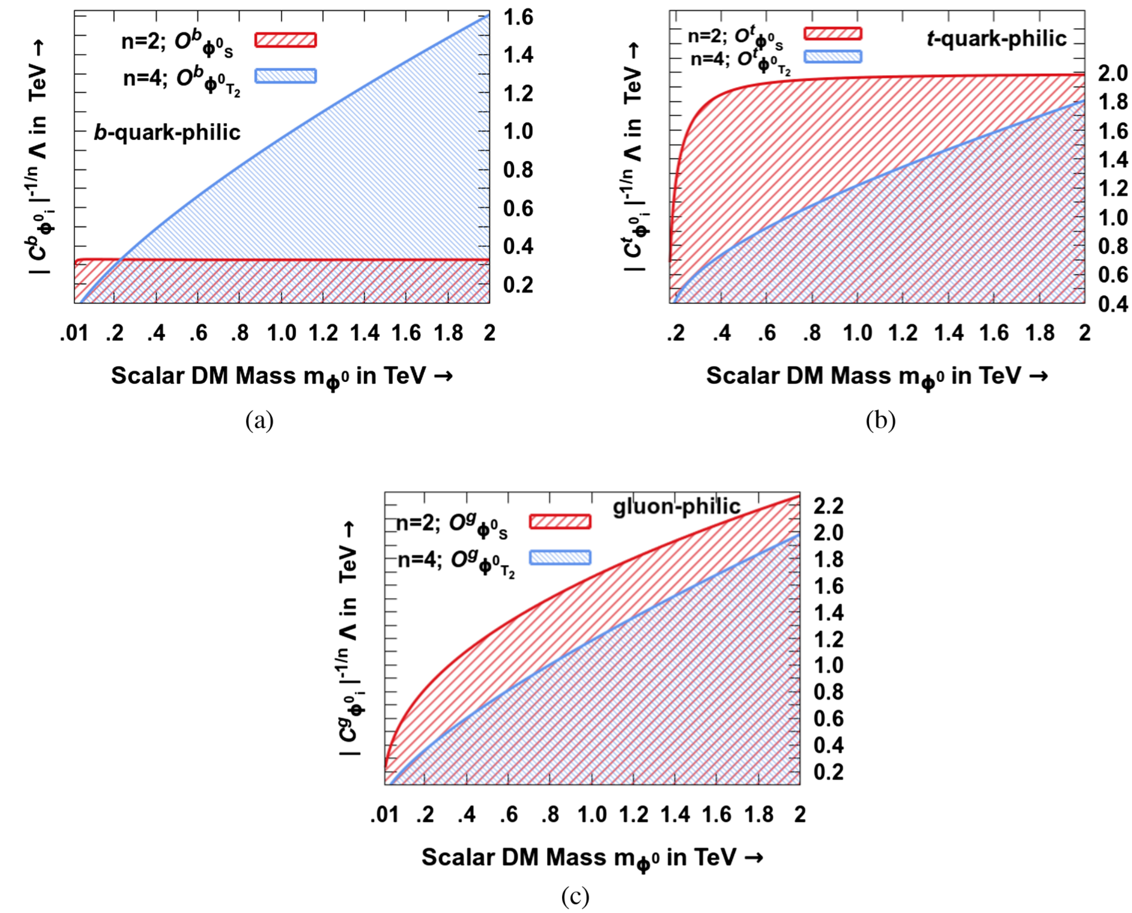

FIG. 2. We depict relic density contours satisfying $\Omega^{\phi^0} h^2 = 0.1198$ [4] and shaded cosmologically allowed regions in the plane defined by Majorana DM mass m_{ϕ^0} and $|C^{q/g}_{\phi^0_{S,T_1}}|^{-1/n}\Lambda$. The b-quarkphilic, t-quarkphilic and gluonphilic scalar DM contours in Figs. 2(a)–2(c) are drawn corresponding to scalar and twist-2 type-2 operators, respectively.

Station, the ground-based Cherenkov telescope H.E.S.S. [17,90–92], HAWC [93–95], and MAGIC [16].

t-quarkphilic DM annihilation yields a pair of $t\bar{t}$, where the $t(\bar{t})$ decays into $b(\bar{b})$ associated with W^+ (W^-) with 100% branching fraction. The charged gauge bosons then decays in either leptonic or semileptonic or hadronic modes. The gluons and/or pair of $b\bar{b}$ produced by DM pair annihilation hadronize partially to neutral pions, which then decay to photon pairs ($\pi^0 \to \gamma\gamma$) with a 99% branching fraction, yielding a broad spectrum of photons. In order to compare the photon spectra observed in FermiLAT [15] and H.E.S.S [17] experiments, the photon flux resulting from the DM pair annihilations is realized by interfacing the MadDM algorithm [82] with the showering and hadronization simulated using PYTHIA 8.0 code [96]. In this subsection, we compare the thermally-averaged DM annihilation cross sections corresponding to the $b\bar{b}$, $t\bar{t}$, and gg channels in the dSphs environment with the upper bounds calculated from the respective recasted experimental limits of the observed photon spectra.

The analytic expressions of thermally-averaged DM pair-annihilation cross sections $\langle\sigma|\vec{v}_{\rm DM}|\rangle$ for Majorana, scalar, and vector DM are given in Appendix B and agree with what is known for other fermions in the literature [40,46,97,98]. These are derived from the cross sections in Appendix A in which the center of mass energy squared s is expanded as $\approx 4m^2_{\rm DM} + m^2_{\rm DM}|\vec{v}_{\rm DM}|^2 + \frac{3}{4}m^2_{\rm DM}|\vec{v}_{\rm DM}|^4 + \mathcal{O}(|\vec{v}_{\rm DM}|^6)$. It is to be noted that DM velocity $|\vec{v}_{\rm DM}|$ is roughly of the order of $\sim 10^{-3}c$ at the center of the Galaxy and $10^{-5}c$ at dSphs in contrast to that of $10^{-1}c$ at freeze-out. In comparison to all chiral blind s-dominated processes, the leading-term contributions from the p-wave and d-wave channels in $\langle\sigma|\vec{v}_{\rm DM}|\rangle$ are proportional to $|\vec{v}_{\rm DM}|^2$ and $|\vec{v}_{\rm DM}|^4$, respectively, and are thus suppressed. This renders the leading p-wave suppressed thermally-averaged DM pair-annihilation cross section to be of the order of 10^{-32} cm^3 s^{-1} in the galactic center and 10^{-36} cm^3 s^{-1} at the dSphs respectively. Henceforth, our the numerical analysis of the leading-order contribution to the velocity dependent/independent thermally-averaged cross sections are performed for dSphs and only those $\langle\sigma|\vec{v}_{\rm DM}|\rangle$ are depicted in the figures which are larger than 10^{-29} cm^3 s^{-1}.

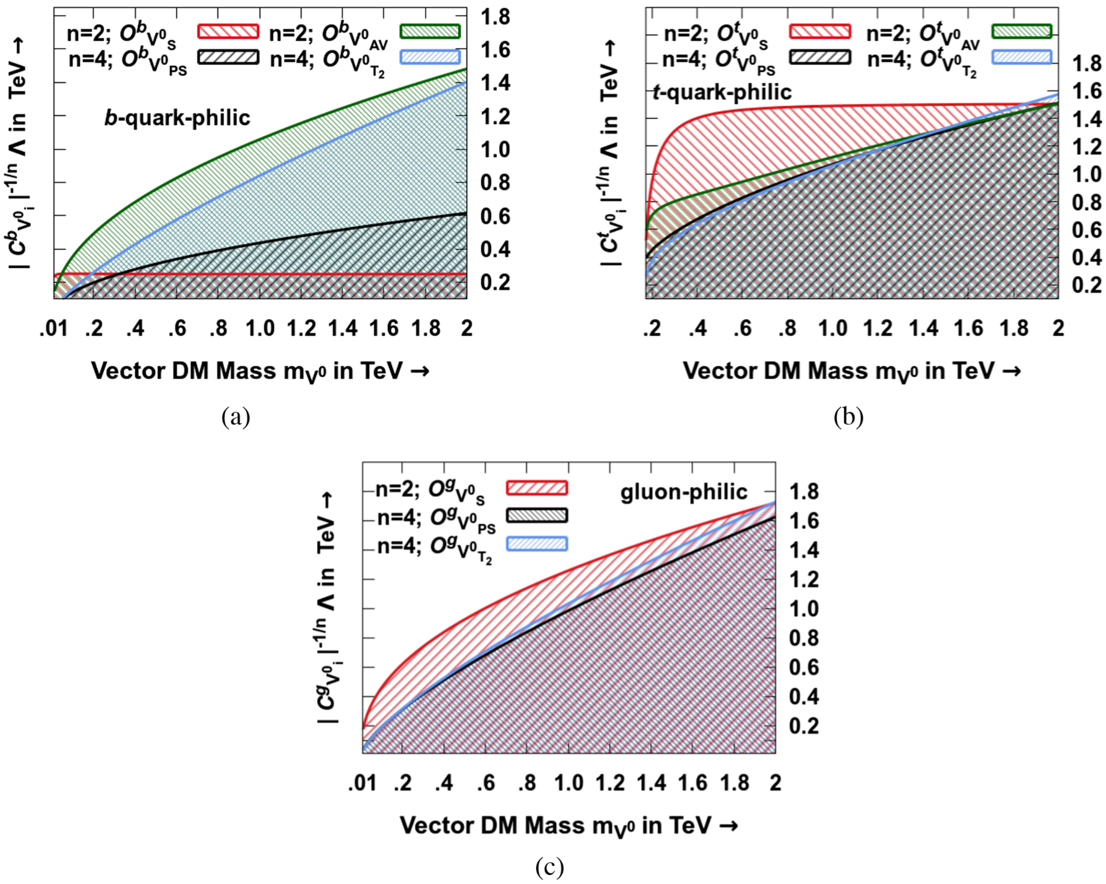

FIG. 3. We depict relic density contours satisfying $\Omega^{V^0} h^2 = 0.1198$ [4] and shaded cosmologically allowed regions in the plane defined by Majorana DM mass m_{V^0} and $|C^{q/g}_{V^0_{\mathrm{S,PS,AV},T_1}}|^{-1/n}\Lambda$. The b-quarkphilic and t-quarkphilic vector DM contours in Figs. 3(a) and 3(b) are drawn corresponding to scalar, pseudoscalar, axial-vector and twist-2 type-2 operators. The gluonphilic vector DM contours for Fig. 3(c) are drawn corresponding to scalar, pseudoscalar, and twist-2 type-2 operators.

For varying m_{DM}, we investigate the contributions to the thermally-averaged DM pair-annihilation cross sections into $b\bar{b}$, $t\bar{t}$, and gg pairs. Using the respective Wilson coefficients satisfying the relic density constraint for a given m_χ as shown in Fig. 1, we calculate and depict the variation of cosmological bound on the thermally-averaged Majorana DM pair-annihilation cross sections with Majorana DM mass for $\chi\bar{\chi} \to b\bar{b}$ and $\chi\bar{\chi} \to t\bar{t}$ in Figs. 4(a) and 4(b) respectively.

We observe that the shape profile of the axial-vector induced contribution to the thermally-averaged DM pair-annihilation cross section with varying DM mass is governed by the term $(1 + \frac{1}{3}\frac{m_\chi^2}{m_f^2}|\vec{v}_\chi|^2 + \cdots)$ in Eq. (B1c), which is approximately ~ 1 for the range of DM masses of phenomenological interest. This is in contrast to the case of relic density computation, where the Wilson coefficient decreases with increasing DM mass to satisfy the relic density constraint. The use of these decreasing constrained couplings with increasing DM masses in Figs. 4(a) and 4(b) is responsible for the negative slope of the $\langle\sigma|\vec{v}_\chi|\rangle$.

In case of the twist-2 type-1 operator the suppression due to increment in the cosmological upper bound on Λ is compensated with the increment in the DM mass alone. The negligible contributions from the heavy-quarkphilic scalar $\mathcal{O}^q_{\chi S}$ operator given in Eq. (B1a) is attributed to the chiral suppression along with DM velocity dependence while gluonphilic scalar $\mathcal{O}^g_{\chi S}$, pseudoscalar $\mathcal{O}^g_{\chi \mathrm{PS}}$, and twist-2 type-1 $\mathcal{O}^g_{\chi T_1}$ operators given in Eqs. (B2a)–(B2c) respectively are p-wave suppressed ($\ll 10^{-29}$ cm^3 s^{-1}) and hence not shown in the graph.

Similarly, we plot the variation of the cosmological bound of the thermally-averaged DM annihilation cross section ($\phi^0\phi^0 \to b\bar{b}/t\bar{t}/gg$) with scalar DM mass m_{ϕ^0} in Fig. 5. The $\langle\sigma|\vec{v}_{\phi^0}|\rangle$ induced by the heavy-quarkphilic twist-2 type-2 operator $\mathcal{O}^q_{\phi^0_{T_2}}$ given in (B3b) is chirally suppressed and therefore falls sharply with an increasing DM mass as shown in Fig. 2. The sharp fall in the t-quarkphilic case, on the other hand, is flattened for DM mass ranges of less than 2 TeV. The gluonphilic twist-2 type-2 operator is d-wave $\propto v^4$ suppressed as shown in Eq. (B4b). Figure 6 shows the thermally-averaged vector DM pair-annihilation cross sections of the third-generation quarks and gluons with varying vector DM

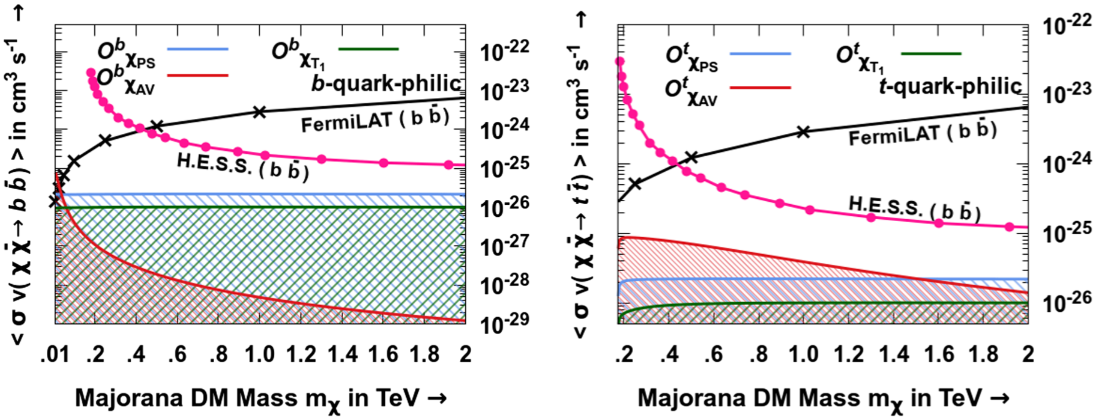

(a) (b)

FIG. 4. Figures 4(a) and 4(b) depict the thermally-averaged cross sections for Majorana DM pair annihilation into $b\bar{b}$ and $t\bar{t}$ pairs, respectively. The contributions from pseudoscalar, axial-vector, and twist-2 type-1 operators in both the panels are evaluated using values for $|C^q_{\chi_{\rm PS,AV,}T_1}/\Lambda^n|$ satisfying $\Omega^\chi h^2 = 0.1198 \pm 0.0012$ [4] as shown in Fig. 1 and hence, the unshaded regions above the respective curves are cosmologically allowed. Regions above the recasted experimental limits obtained from FermiLAT [15] as well as H.E.S.S. [17] are excluded.

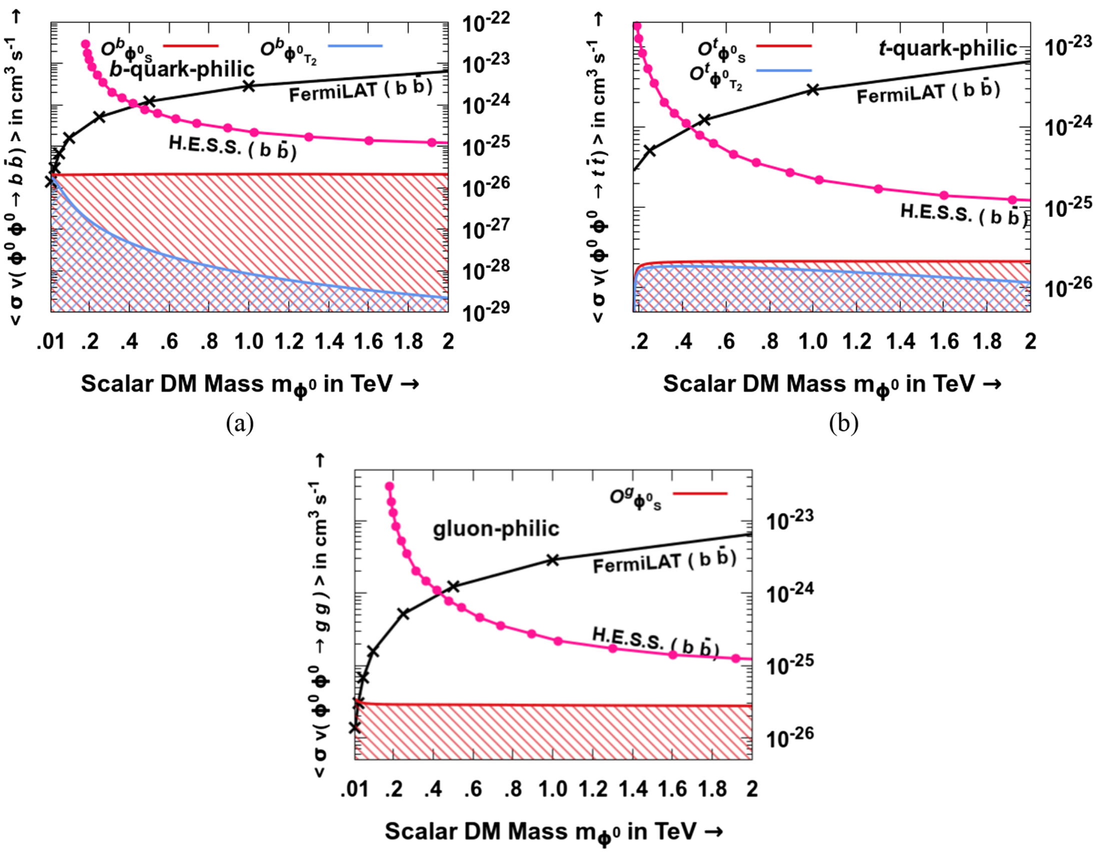

(a) (b)

(c)

FIG. 5. Figures 5(a)–5(c) depict the thermally-averaged cross sections for real scalar DM pair annihilation into $b\bar{b}$, $t\bar{t}$, and gg pairs, respectively. The contributions from scalar and twist-2 type-2 operators in the panels are evaluated using their respective values for $|C^{q,g}_{\phi^0_{S,T_2}}/\Lambda^n|$ satisfying $\Omega^{\phi^0} h^2 = 0.1198 \pm 0.0012$ [4] as shown in Fig. 2 and hence, the unshaded regions above the respective curves are cosmologically allowed. Regions above the recasted experimental limits obtained from FermiLAT [15] as well as H.E.S.S. [17] are excluded.

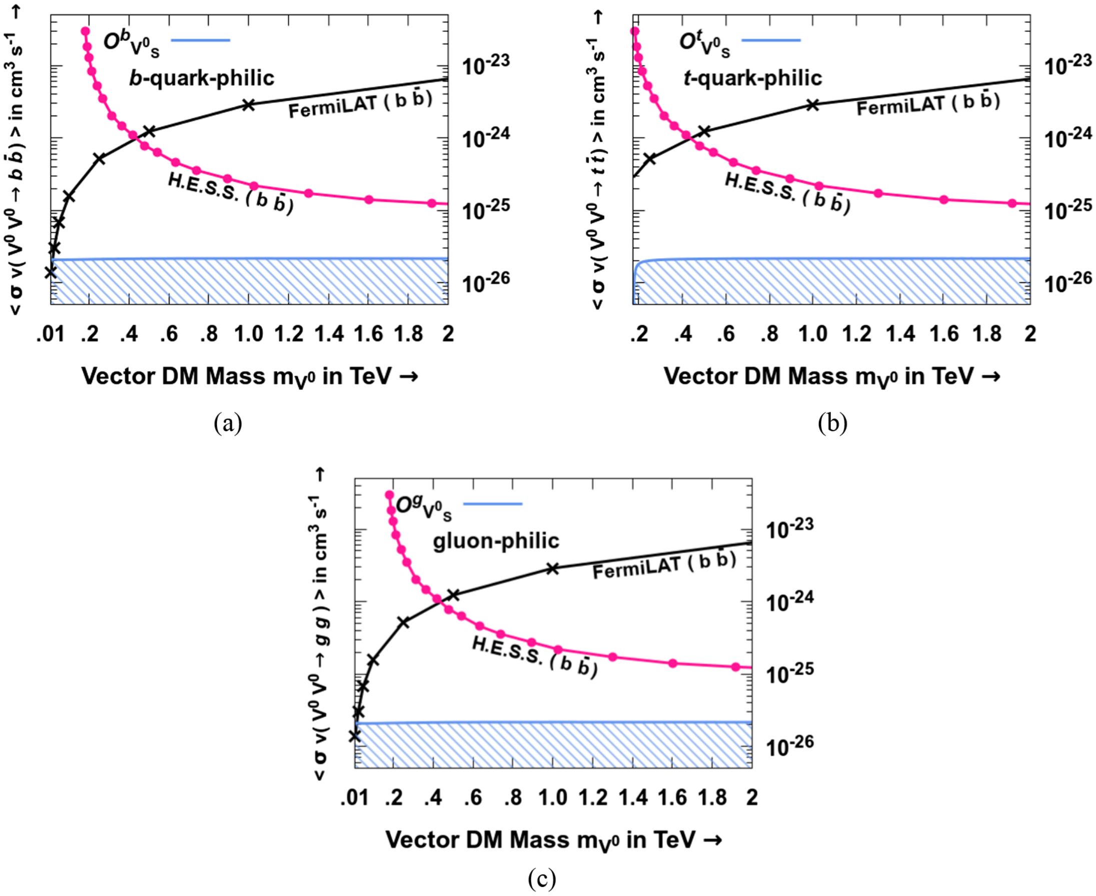

FIG. 6. Figures 6(a)–6(c) depict the thermally averaged cross sections for real vector DM pair annihilation into $b\bar{b}$, $t\bar{t}$, and gg pairs, respectively. The contributions from scalar and pseudoscalar operators in the panels are evaluated using their respective values for $|C^{q,g}_{V^0_{S/PS}}/\Lambda^n|$ satisfying $\Omega^{V^0}h^2 = 0.1198 \pm 0.0012$ [4] as shown in Fig. 3 and hence, the unshaded regions above the respective curves are cosmologically allowed. Regions above the experimental limits obtained from the recasted FermiLAT [15] as well as H.E.S.S. [17] are excluded.

mass corresponding to the respective cosmological bound on the Wilson coefficient as shown in Fig. 3. Unlike the chiral p-wave suppressed pseudoscalar and axial-vector operators and d-wave suppressed twist-2 type-2 operators, we observe an appreciable contribution to the $\langle\sigma|\vec{v}_{V^0}|\rangle$ from the heavy-quarkphilic and gluonphilic scalar operators which are of the order of $\sim 10^{-26}$ cm^3 s^{-1}.

C. DM-nucleon scattering

In direct detection experiments, the scattering of DM particles can be broadly classified as (a) DM-electron scattering, (b) DM-atom scattering, and (c) DM-nucleon scattering. In the absence of heavy sea quarks and antiquarks inside nucleons at the direct detection energy scale, the b-quarkphilic and t-quarkphilic DM interacts with the constituent gluons via a loop, as shown in Fig. 7.

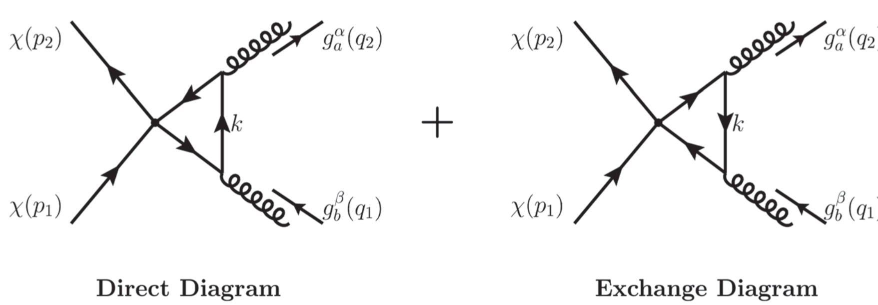

FIG. 7. One-loop Majorana DM gluon scattering diagrams where the blob represents the four fermionic effective interactions induced by the scalar/axial-vector/twist-2 currents of heavy quarks.

We compute the dominant DM-gluon one-loop elastic scattering amplitudes induced by the scalar, axial-vector, and twist-2 point interactions among DM and heavy quarks. The mass scale m_Q of the heavy quarks running in the loop and the QCD coupling strength α_s characterize the loop amplitudes. We derive the phenomenological effective DM gluon-interaction Lagrangians given in (C1a)–(C1c) which correspond to Majorana, real scalar, and real vector DM candidates, respectively.

Since the nonrelativistic DM particles scatter the nucleons and not the free gluons, we perform the nonrelativistic reduction of the interaction Lagrangian given in Appendix C. We connect the DM-gluon amplitudes induced by the scalar and twist-2 currents of heavy quarks at one-loop order with their respective DM-effective nucleon interactions by evaluating the expectation values of the zero-momentum scalar and twist-2 gluonphilic operators between the initial and final nucleons in Eqs. (C3) and (C5), respectively. The Majorana, real scalar, and real vector DM-nucleon scattering cross sections driven by the heavy-quark scalar, axial-vector, and twist-2 currents are given as

$$\sigma_{\rm S}^{q^{\chi N}} = \frac{8}{81}\frac{1}{\pi}(C^q_{\chi_S})^2\left[\frac{1\ \mathrm{TeV}}{\Lambda}\right]^6\left[\frac{m_N}{1\ \mathrm{GeV}}\right]^2\left[\frac{\mu_{N\chi}}{1\ \mathrm{GeV}}\right]^2\left[\frac{\alpha_s(\Lambda)}{\alpha_s(\mu)}\right]^2 \times |I_S^{gg}|^2|f_{\rm TG}^N|^2(3.9\times10^{-46})\ \mathrm{cm}^2, \tag{12a}$$

$$\sigma_{\rm AV}^{q^{\chi N}} = \frac{16}{3}\frac{1}{\pi}(C^q_{\chi_{\rm AV}})^2\left[\frac{1\,\mathrm{TeV}}{\Lambda}\right]^4\left[\frac{\mu_{N\chi}}{1\,\mathrm{GeV}}\right]^2\left[\frac{\alpha_s(\Lambda)}{\alpha_s(\mu)}\right]^2 \times\left[\frac{175\,\mathrm{GeV}}{m_Q}\right]^4|I_{\rm AV}^{gg}|^2\left[\frac{|\vec{q}|}{10\,\mathrm{MeV}}\right]^4\left[\sum_{q=u,d,s}\Delta_q^{(N)}\frac{\bar{m}}{m_q}\right]^2 \times\left[\frac{\mathcal{J}+1}{\mathcal{J}}\right]S_N S'_N(4.13\times10^{-57})\,\mathrm{cm}^2, \tag{12b}$$

$$\sigma_{\rm T}^{q^{\chi N}} = \frac{2}{\pi}(C^q_{\chi_T})^2\left[\frac{1\ \mathrm{TeV}}{\Lambda}\right]^8\left[\frac{\alpha_s(\Lambda)}{4\pi}\right]^2\left[\frac{\mu_{\chi N}}{1\ \mathrm{GeV}}\right]^2\left[\frac{M_\chi}{100\ \mathrm{GeV}}\right]^2 \times\left[\frac{m_N}{1\ \mathrm{GeV}}\right]^2\left[\ln\left(\frac{\Lambda^2}{m_Q^2}\right)\right]^2|(g(2;\Lambda)|^2 \times(1.98\times10^{-48})\ \mathrm{cm}^2, \tag{12c}$$

$$\sigma_S^{q^{\phi^0 N}} = \frac{4}{81}\frac{1}{\pi}(C^q_{\phi^0_S})^2\left[\frac{1\ \mathrm{TeV}}{\Lambda}\right]^4\left[\frac{100\ \mathrm{GeV}}{m_{\phi^0}}\right]^2\left[\frac{m_N}{1\ \mathrm{GeV}}\right]^2 \times\left[\frac{\mu_{N\chi}}{1\ \mathrm{GeV}}\right]^2\left[\frac{\alpha_s(\Lambda)}{\alpha_s(\mu)}\right]^2 \times|I_S^{gg}|^2|f_{\rm TG}^N|^2(3.9\times10^{-44})\ \mathrm{cm}^2, \tag{13a}$$

$$\sigma_{T_2}^{q^{\phi^0 N}} = \frac{1}{2\pi}(C^q_{\phi^0_{T_2}})^2\left[\frac{1\ \mathrm{TeV}}{\Lambda}\right]^8\left[\frac{\alpha_s(\Lambda)}{4\pi}\right]^2\left[\frac{\mu_{\phi^0 N}}{1\ \mathrm{GeV}}\right]^2 \times\left[\frac{M_{\phi^0}}{100\ \mathrm{GeV}}\right]^2\left[\frac{m_N}{1\ \mathrm{GeV}}\right]^2\left[\ln\left(\frac{\Lambda^2}{m_Q^2}\right)\right]^2 \times|g(2;\Lambda)|^2(1.98\times10^{-48})\ \mathrm{cm}^2, \tag{13b}$$

$$\sigma_S^{q^{V^0 N}} = \frac{4}{243}\frac{1}{\pi}(C^q_{V^0_S})^2\left[\frac{1\ \mathrm{TeV}}{\Lambda}\right]^4\left[\frac{100\ \mathrm{GeV}}{m_{V^0}}\right]^2 \times\left[\frac{m_N}{1\ \mathrm{GeV}}\right]^2\left[\frac{\mu_{N\chi}}{1\ \mathrm{GeV}}\right]^2\left[\frac{\alpha_s(\Lambda)}{\alpha_s(\mu)}\right]^2 \times|I_S^{gg}|^2|f_{\rm TG}^N|^2(3.9\times10^{-44})\ \mathrm{cm}^2, \tag{14a}$$

$$\sigma_{\rm AV}^{q^{V^0 N}} = \frac{32}{9}\frac{1}{\pi}(C^q_{V^0_{\rm AV}})^2\left[\frac{1\ \mathrm{TeV}}{\Lambda}\right]^4\left[\frac{\mu_{NV^0}}{1\ \mathrm{GeV}}\right]^2\left[\frac{\alpha_s(\Lambda)}{\alpha_s(\mu)}\right]^2 \times\left[\frac{175\ \mathrm{GeV}}{m_Q}\right]^4|I_{\rm AV}^{gg}|^2\left[\frac{|\vec{q}|}{10\ \mathrm{MeV}}\right]^4 \times\left[\sum_{q=u,d,s}\Delta_q^{(N)}\frac{\bar{m}}{m_q}\right]^2\left[\frac{\mathcal{J}+1}{\mathcal{J}}\right] \times S_N S'_N(4.13\times10^{-57})\ \mathrm{cm}^2, \tag{14b}$$

$$\sigma_{T_2}^{q^{V^0 N}} = \frac{1}{6\pi}(C^q_{V^0_{T_2}})^2\left[\frac{1\ \mathrm{TeV}}{\Lambda}\right]^8\left[\frac{\alpha_s(\Lambda)}{4\pi}\right]^2 \times\left[\frac{\mu_{V^0 N}}{1\ \mathrm{GeV}}\right]^2\left[\frac{M_{V^0}}{100\ \mathrm{GeV}}\right]^2\left[\frac{m_N}{1\ \mathrm{GeV}}\right]^2 \times\left[\ln\left(\frac{\Lambda^2}{m_Q^2}\right)\right]^2|g(2;\Lambda)|^2\times(1.98\times10^{-48})\ \mathrm{cm}^2, \tag{14c}$$

where $\mu_{N\mathrm{DM}} \equiv (m_N m_{\rm DM})/(m_N + m_{\rm DM})$ is the reduced mass for the respective DM-nucleon system and the scale μ is taken to be Z^0-boson mass. For the computation of scale-dependent $\alpha_s(\mu)$, $\alpha_s(\Lambda)$, and $g(x;\Lambda)$, we access CTEQ6l1 [99] PDF data set from the LHAPDF6 [100] library. However, the scale dependence of the Wilson coefficients is found to be smaller than that of α_s, as noted by the authors of the Ref. [101]. It is to be noted that the observed logarithmically enhanced one-loop induced scattering cross sections in Eqs. (12c), (13b), and (14c) result from the explicit momentum dependence in the twist-2 operator interaction Lagrangian given in Eqs. (3), (6), and (8), respectively. The real vector DM-nucleon scattering cross sections driven by the scalar and twist-2 type-2 currents of heavy quarks in Eqs. (14a) and (14c) respectively are found to be $1/3$ of the scalar DM-nucleon scattering cross sections corresponding to scalar and twist-2 type-2 currents of heavy quarks in Eqs. (13a) and (13b), respectively. The velocity suppressed spin-dependent DM-nucleon scattering events induced by the pseudoscalar operators are not analyzed.

For completion, we compute and display the tree-level spin-independent Majorana DM nucleon, scalar DM nucleon, and vector DM nucleon-scattering cross sections induced by the scalar and twist-2 current of gluons in Eqs. (15a)–(15b), (16a)–(16b), and (17a)–(17b), respectively as

$$\sigma_S^{g^{\chi N}} = \frac{128}{81}\frac{1}{\pi}(C^g_{\chi_S})^2\left[\frac{1\ \text{TeV}}{\Lambda}\right]^8\left[\frac{m_\chi}{100\ \text{GeV}}\right]^2\left[\frac{m_N}{1\ \text{GeV}}\right]^2 \times\left[\frac{\mu_{N\chi}}{1\ \text{GeV}}\right]^2\left[\frac{\alpha_s(\Lambda)}{\alpha_s(\mu)}\right]^2|f^N_{\text{TG}}|^2\times(3.9\times10^{-48})\ \text{cm}^2, \tag{15a}$$

$$\sigma_{T_1}^{g^{\chi N}} = \frac{9}{8}\frac{1}{\pi}(C^g_{\chi_{T_1}})^2\left[\frac{1\,\text{TeV}}{\Lambda}\right]^8\left[\frac{m_\chi}{100\,\text{GeV}}\right]^2\left[\frac{m_N}{1\,\text{GeV}}\right]^2\left[\frac{\mu_{N\chi}}{1\,\text{GeV}}\right]^2 \times|g(2;\mu_F)|^2\times(3.9\times10^{-48})\,\text{cm}^2, \tag{15b}$$

$$\sigma_S^{g^{\phi^0 N}} = \frac{64}{81}\frac{1}{\pi}(C^g_{\phi^0_S})^2\left[\frac{1\ \text{TeV}}{\Lambda}\right]^4\left[\frac{100\ \text{GeV}}{m_{\phi^0}}\right]^2 \times\left[\frac{m_N}{1\ \text{GeV}}\right]^2\left[\frac{\mu_{N\phi^0}}{1\ \text{GeV}}\right]^2\left[\frac{\alpha_s(\Lambda)}{\alpha_s(\mu)}\right]^2 \times|f^N_{\text{TG}}|^2(3.9\times10^{-44})\ \text{cm}^2, \tag{16a}$$

$$\sigma_{T_2}^{g^{\phi^0 N}} = \frac{9}{32\pi}(C^g_{\phi^0_{T_2}})^2\left[\frac{1\ \text{TeV}}{\Lambda}\right]^8\left[\frac{\alpha_s(\Lambda)}{4\pi}\right]^2 \times\left[\frac{\mu_{N\phi^0}}{1\ \text{GeV}}\right]^2\left[\frac{m_{\phi^0}}{100\ \text{GeV}}\right]^2\left[\frac{m_N}{1\ \text{GeV}}\right]^2 \times|g(2;\mu_F)|^2(3.9\times10^{-48})\ \text{cm}^2, \tag{16b}$$

$$\sigma_S^{g^{V^0 N}} = \frac{64}{243}\frac{1}{\pi}(C^g_{V^0_S})^2\left[\frac{1\ \text{TeV}}{\Lambda}\right]^4\left[\frac{100\ \text{GeV}}{m_{V^0}}\right]^2 \times\left[\frac{m_N}{1\ \text{GeV}}\right]^2\left[\frac{\mu_{NV^0}}{1\ \text{GeV}}\right]^2\left[\frac{\alpha_s(\Lambda)}{\alpha_s(\mu)}\right]^2 \times|f^N_{\text{TG}}|^2(3.9\times10^{-44})\ \text{cm}^2, \tag{17a}$$

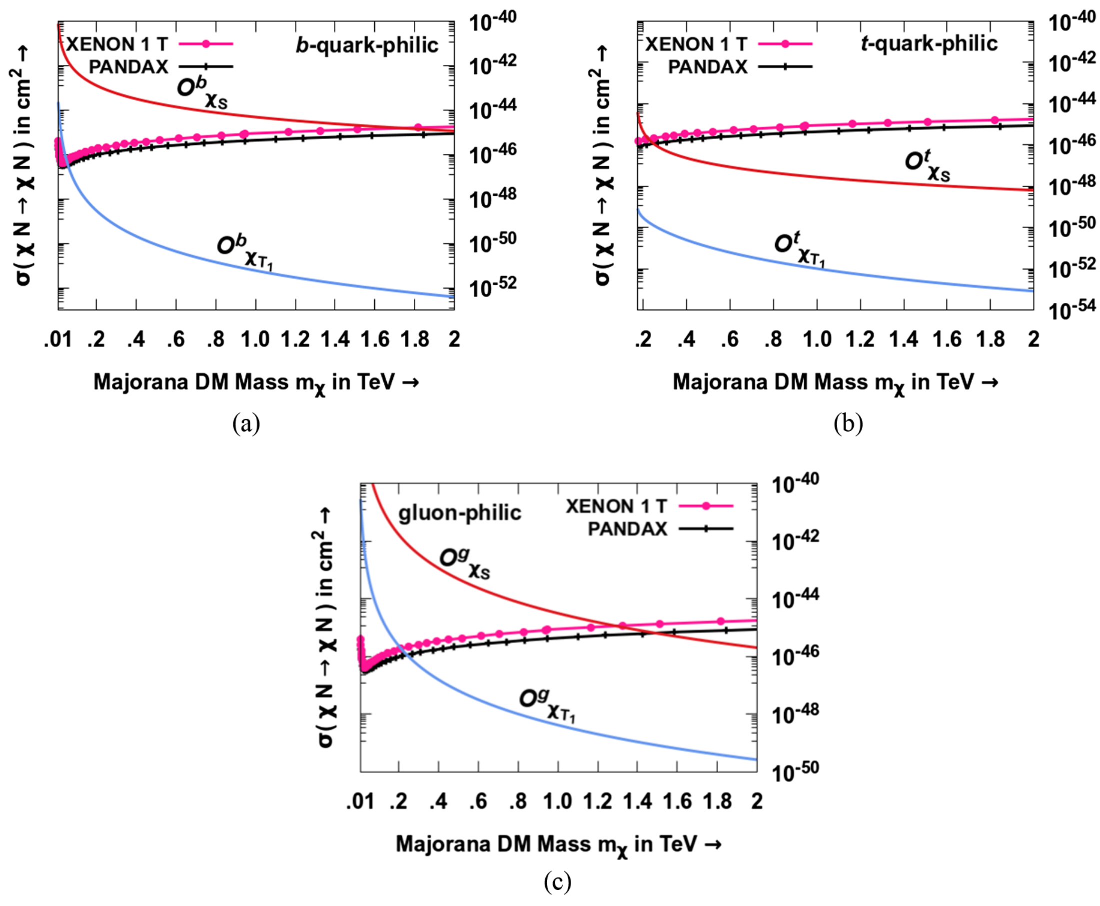

FIG. 8. Figures 8(a)–8(c) depict the spin-independent b-quark, t-quark, and gluonphilic Majorana DM-nucleon scattering cross sections respectively. The scalar and twist-2 type-1 contributions in all panels are evaluated using their respective values for $|C^{q,g}_{\chi_{S,T_1}}/\Lambda^n|$ satisfying $\Omega^\chi h^2 = 0.1198 \pm 0.0012$ [4] as shown in Fig. 1 and hence, regions above the solid curves are cosmologically allowed. Regions above the experimental limits obtained from XENON-1T [6] and PandaX-4T [8] are excluded.

$$\sigma_{T_2}^{g^{V^0 N}} = \frac{3}{32\pi}(C^g_{V^0_{T_2}})^2 \left[\frac{1\ \text{TeV}}{\Lambda}\right]^8 \left[\frac{\alpha_s(\Lambda)}{4\pi}\right]^2 \times \left[\frac{\mu_{NV^0}}{1\ \text{GeV}}\right]^2 \left[\frac{m_{V^0}}{100\ \text{GeV}}\right]^2 \left[\frac{m_N}{1\ \text{GeV}}\right]^2 \times |g(2;\mu_F)|^2 (3.9\times 10^{-48})\ \text{cm}^2. \tag{17b}$$

The analytical expressions for the gluonphilic DM-nucleon scattering cross sections are in agreement with those given in Ref. [74].

We display the spin-independent Majorana, real scalar and real vector DM-nucleon scattering cross sections with respect to DM mass in Figs. 8–10, respectively. The scalar and twist-2 currents induced by b-quarkphilic and t-quarkphilic DM interactions are depicted in the left and right panels of all the three figures. Since, the cross sections are evaluated using the Wilson coefficients obtained from the relic density contours satisfying $\Omega^{\rm DM} h^2 = 0.1198$ in Figs. 1–3 for the Majorana, scalar and vector DM respectively, the solid curves represent the cosmological lower limits of the scattering cross sections.

Each panel in Figs. 8–10 also display the central values of the spin-independent cross sections for a given DM mass from the interpolation of the observed data in XENON-1T [6] and PandaX-4T data [8] experiments. The data for these cross sections is derived from the lack of any excess in the aforementioned experiments using statistical analysis of the recoil energy spectrum in the binned likelihood approach. These curves from the experiments determine the upper limit of direct detection spin-independent cross section. As a result, the experimental upper bound validates the region between the experimental upper bound and the specific cosmological lower limit curve, where the relic density constraint was satisfied using the corresponding fixed Wilson coefficient.

The profile of the spin-dependent DM-nucleon scattering cross sections induced by the axial-vector coupling of heavy quarks with Majorana and vector DM is characterized by their respective DM-gluon effective pseudoscalar interaction Lagrangians given in Eqs. (C1a) and (C1c) respectively. Due to the entangled momentum dependency of the cross section inside the velocity integral in the

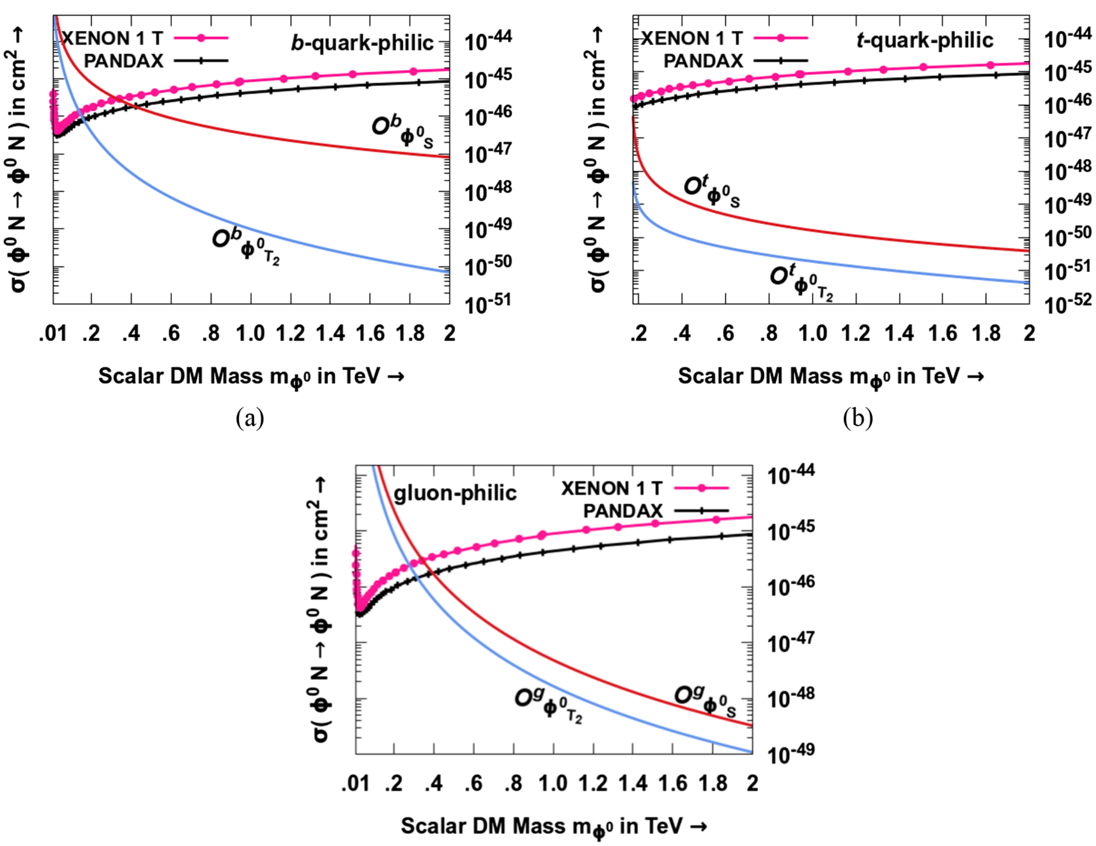

FIG. 9. Figures 9(a)–9(c) depict the spin-independent b-quark, t-quark, and gluonphilic scalar DM-nucleon scattering cross sections, respectively. The scalar and twist-2 type-2 contributions in all the panels are evaluated using their respective values for $|C^{q,g}_{\phi^0_{S,T_2}}/\Lambda^n|$ satisfying $\Omega^{\phi^0} h^2 = 0.1198 \pm 0.0012$ [4] as shown in Fig. 2 and hence, regions above the solid curves are cosmologically allowed. Regions above the experimental limits obtained from XENON-1T [6] and PandaX-4T [8] are excluded.

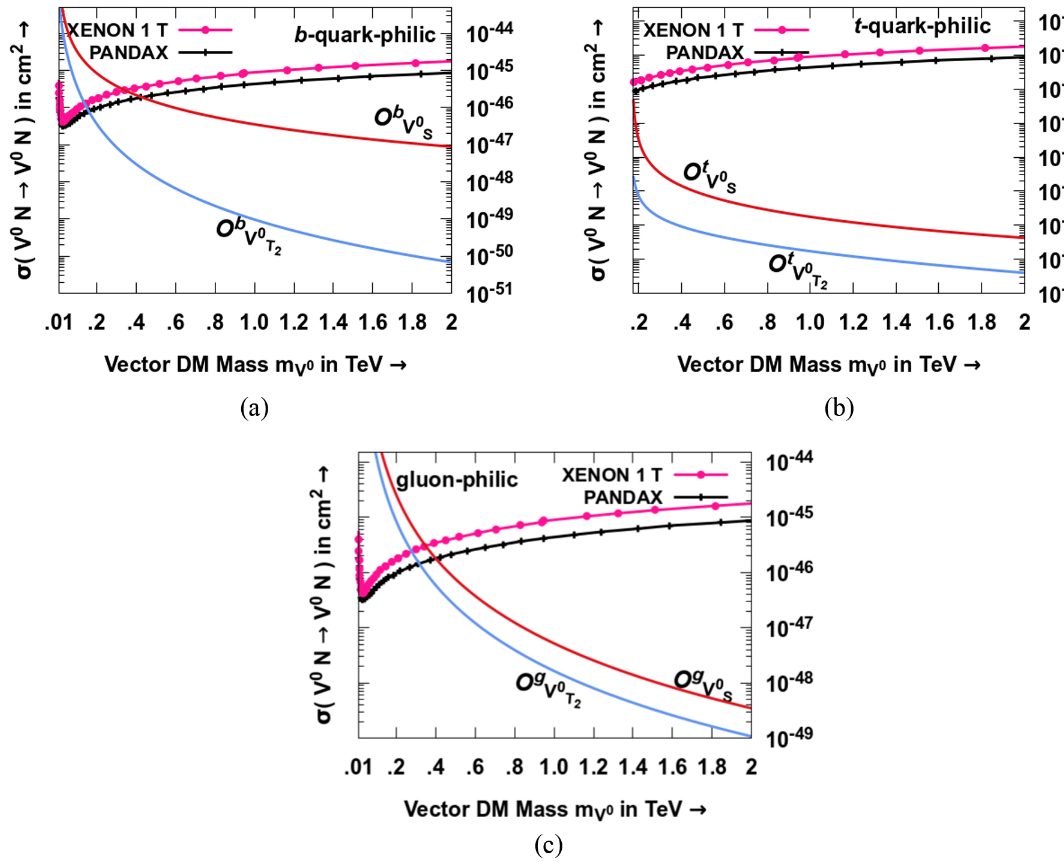

FIG. 10. Figures 10(a)–10(c) depict the spin-independent b-quark, t-quark, and gluonphilic vector DM-nucleon scattering cross sections, respectively. The scalar and twist-2 type-2 contributions in all the panels are evaluated using their respective values for $|C^{q,g}_{V^0_{S,T_2}}/\Lambda^n|$ satisfying $\Omega^{V^0}h^2 = 0.1198 \pm 0.0012$ [4] as shown in Fig. 3 and hence, regions above the solid curves are cosmologically allowed. Regions above the experimental limits obtained from XENON-1T [6] and PandaX-4T [8] are excluded.

event-rate calculation, an exclusive numerical estimation of the scattering cross section corresponding to such operator is beyond the scope of our analysis. The upper limits on Wilson coefficients corresponding to the effective spin and momentum dependent pseudoscalar interaction of gluons with fermionic DM have been extracted by interpolating the data for event rates from the experimental data in Refs. [102,103] for $m_{\rm DM}$ less than 1 TeV.

1. Nuclear recoil spectrum

For a fixed target detector exposure ϵ_T and target nucleus mass $m_{\rm nuc}$., the differential nuclear recoil event rate with respect to nuclear recoil energy $dR_{\rm nuc}/dE_r$ corresponding to the DM-nucleon scattering cross section σ_N and DM velocity $|\vec{v}|$ is given as

$$\begin{aligned}\frac{dR_{\rm nuc}}{dE_{\rm r}} &= \frac{\epsilon_T\rho_0}{m_{\rm nuc}m_{\rm DM}}\int_{|\vec{v}|_{\rm min}}^{|\vec{v}_{\rm esc}|}|\vec{v}|f(|\vec{v}|)\frac{d\sigma}{dE_{\rm r}}d|\vec{v}| \\ &= \frac{\epsilon_T\rho_{\rm DM}}{2m_{\rm DM}}\frac{\sigma_N A^2}{\mu_N^2}|F(|\vec{q}|r_n)|^2\int_{|\vec{v}|_{\rm min}}^{|\vec{v}|_{\rm max}}\frac{1}{|\vec{v}_{\rm DM}|}f(|\vec{v}|)d^3\vec{v}, \end{aligned} \tag{18}$$

where $F(|\vec{q}|r_n)$ is the Helm form factor taking account of the nonvanishing finite size of the nucleus [104]. Here $r_n \equiv 1.2\times A^{1/3}$ is the effective radius of the nucleus with atomic mass A and $|\vec{q}|$ is the momentum transfer corresponding to the recoil energy E_r. Following Ref. [105], the velocity integral for normalized Maxwellian DM velocity distribution is solved as

$$\begin{aligned}\int_{|\vec{v}|_{\rm min}}^{|\vec{v}|_{\rm max}}\frac{f(|\vec{v}|)}{|\vec{v}|}d^3\vec{v} &= \int_{\sqrt{m_{\rm nuc}E_r/(2\mu_{\rm nuc}^2)}}^{|\vec{v}_{\rm esc}|}\frac{1}{|\vec{v}|}e^{-[(|\vec{v}+\vec{v}_E|)/|\vec{v}_0|]^2}d^3\vec{v} \\ &= \frac{1}{2|\vec{v}_E|}{\rm erf}(\eta_-,\eta_+) \\ &\quad -\frac{1}{\pi|\vec{v}_E|}(\eta_+-\eta_-)e^{-[|\vec{v}_{\rm esc}|/|\vec{v}_0|]^2}, \quad \text{where}\end{aligned} \tag{19a}$$

$$\eta_\pm = \min\left[\frac{\sqrt{m_{\rm nuc}E_r/(2\mu_{\rm nuc}^2)}\pm|\vec{v}_E|}{|\vec{v}_0|},\frac{|\vec{v}_{\rm esc}|}{|\vec{v}_0|}\right] \quad \text{and}$$

$$\mu_{\rm nuc} \equiv \frac{m_{\rm DM}m_{\rm nuc}}{m_{\rm DM}+m_{\rm nuc}}. \tag{19b}$$

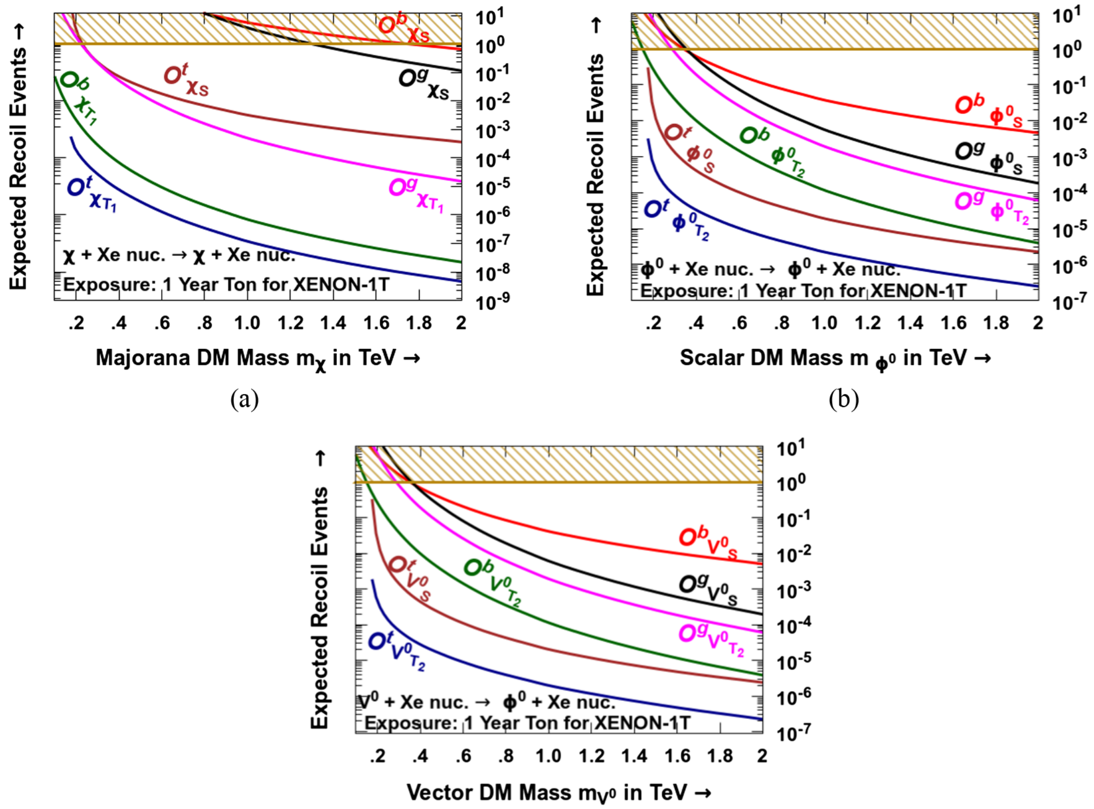

(c)

FIG. 11. Figures 11(a)–11(c) depict the spin-independent recoiled nucleus event due to respective scattering of Majorana, scalar and vector DM with Xe nucleus. The scalar and twist-2 interactions of b-quark, t-quark and gluon in all the three panels are evaluated using their respective values for $|C^{q,g}_{\chi_{S,T_1}}/\Lambda^n|$, $|C^{q,g}_{\phi^0_{S,T_2}}/\Lambda^n|$ and $|C^{q,g}_{V^0_{S,T_2}}/\Lambda^n|$ satisfying $\Omega^{\rm DM}h^2 = 0.1198 \pm 0.0012$ [4] as shown in Figs. 1–3, respectively and hence, regions above the solid curves are cosmologically allowed. The shaded region is excluded from XENON-1T data.

For numerical computation we have taken the Earth's velocity relative to the Galactic frame to be $|\vec{v}_E| = 232\,\text{km/s}$, $|\vec{v}_0| = 220$ km/s and the escape velocity $|\vec{v}_{\rm esc}| = 544\,\text{km/s}$. Further, in order to incorporate the detector-based effects, the nucleus recoil event rate $dR_{\rm nuc}/dE_r$ is convoluted with the detector efficiency [6]. Integrating over the recoil energy from $E_{\rm th} \sim 4.9$ KeV to the maximum $E_{\rm max}$ for a fixed duration and size of the detector, we can estimate the expected recoil nucleus events.

As an illustration, we predict and plot the probable number of Xe nuclear recoil events with respect to varying DM masses in a XENON-1T [6] setup where 1.3 tonnes of Xe target are exposed for a duration of 278.8 days, which is equivalent to one Ton year of net target exposure.

The expected number of recoil nucleus events due to Majorana DM-Xe nucleus scattering, scalar DM-Xe nucleus scattering, and vector DM-Xe nucleus scattering, respectively, are depicted in Figs. 11(a)–11(c), which are induced by scalar and twist-2 currents of heavy quarks at the one-loop level and of gluons at tree level. Since the solid curves in the figures are created with the corresponding lower bound on the Wilson coefficients satisfying the relic density restriction $\Omega^{\rm DM}h^2 = 0.1198$, they correspond to the fixed number of events. This results in lower limits on the estimated number of recoil nucleus events for a particular DM mass. The regions above the respective curves are cosmologically permissible.

The upper bound on the spin-independent scattering events corresponding to the central value of the upper bound obtained in the direct detection cross section for the XENON-1T experiment [6] is then compared with the theoretical predictions for the event rate with fixed Wilson coefficients in each panel of Figs. 11(a)–11(c). We find that the XENON-1T experiment rules out the contributions of b-quarkphilic and gluonphilic Majorana DM scalar interactions for $m_\chi \leq 1.8$ and 1.3 TeV, respectively. Barring the said two operators, we find that contributions from all other operators pertaining to Majorana, scalar and vector DM for $m_{\rm DM} \geq 200$ GeV may be probed in the ongoing and future direct detection experiments with enhanced target exposure.

IV. SUMMARY AND CONCLUSIONS

In this article we assess the viability of the b-quarkphilic, t-quarkphilic, and gluonphilic self-conjugated spin 1/2, 0, and 1 DM candidates in the EFT approach. We have formulated the generalized effective interaction Lagrangian induced by the scalar, pseudoscalar, axial-vector, and twist-2 operators for the real particles in Sec. II.

For a given DM mass, the relic abundance of Majorana, scalar, and vector DM is computed in Sec. III A using the thermally averaged cross sections in Appendix B. Figures 1–3 show 28 interaction strengths in the form of Wilson coefficients $|C^{q,g}_{\mathrm{DM}_i O_j}/\Lambda^n|$ in TeV^{-n} (11 for Majorana DM, six for scalar DM and 11 for vector DM) satisfying the relic density constraint $\Omega^{\mathrm{DM}} h^2 \approx 0.1198$ [4].

Using the constrained Wilson coefficients, we study the thermally-averaged DM pair-annihilation cross sections for the indirect detection of varying DM masses (0.01–2 TeV) in Figs. 4–6. The contributions driven by the lower limit of the effective couplings to the annihilation cross sections in $b\bar{b}$, $t\bar{t}$, and gg channels are found to be consistent when compared with the upper limits of the $b\bar{b}$-annihilation cross sections obtained from FermiLAT [15] and H.E.S.S. [17] indirect experiments.

The scattering of the incident heavy-quarkphilic DM particle off the static nucleon induced by the effective one-loop interactions of the Majorana/scalar/vector DM with gluons in the direct detection experiments are studied. The contributions of gluonphilic Majorana, scalar, and vector DM are revisited and found to be in agreement with results in the literature [74]. Lower bounds on the dominant spin-independent scalar and twist currents induced scattering cross sections are derived by switching the respective cosmological lower limits on Wilson coefficients one by one for Majorana, scalar, and vector DM, as illustrated in Figs. 8–10. They are compared with the available results from XENON-1T [6] and PandaX-4T [8]. Furthermore, with an identical target exposure of one tonne per year in the XENON-1T experiment, we compute the lower bound on the predicted number of recoil nucleus events due to Majorana, scalar and vector DM nucleon scattering and are shown in Figs. 11(a)–11(c).

Finally, Figs. 12–14 corresponding to real spin 1/2, 0, and 1 DM candidates, respectively encapsulate the predicted range for the 18 Wilson coefficients associated with scalar and twist-2 operators when activated individually. The cosmological relic density [4] puts the lower bounds on the Wilson coefficients for varying DM mass $\sim 0.01 \le m_{\mathrm{DM}} \le 2$ TeV, while the upper limits on spin-independent scattering cross sections obtained in the XENON-1T direct detection experiment [6] puts the upper bounds on the Wilson coefficients. However, with the simultaneous switching of these operators the shaded allowed band of the Wilson coefficients shown in Figs. 12–14 may shift below. Findings of our analysis are summarized as follows:

(a) Contributions from b-quarkphilic, t-quarkphilic, and gluonphilic Majorana DM scalar operators are found to be viable solutions for $m_\chi \ge 1.8$ TeV, 200 GeV, and 1.25 TeV, respectively, as shown in Fig. 12(a). The contributions of b-quarkphilic, t-quarkphilic, and gluonphilic twist-2 type-1 Majorana DM operators shown in Fig. 12(b) have been validated for a much wider spectrum of $m_\chi \ge 60$ GeV, 200 GeV, and 200 GeV, respectively.

(b) In Fig. 13(a) contributions from b-quarkphilic, t-quarkphilic, and gluonphilic scalar DM scalar operators are found to be consistent with current experimental data for $m_{\phi^0} \ge 350$ GeV, 200 GeV, and 350 GeV, respectively. The corresponding contributions induced by twist-2 type-2 DM operators are validated for $m_{\phi^0} \ge 150$ GeV, 200 GeV, and 280 GeV, respectively as shown in the Fig. 13(b).

(c) In Fig. 14(a) contributions from b-quarkphilic, t-quarkphilic, and gluonphilic vector DM scalar operators are validated for $m_{V^0} \ge 350$ GeV, 180 GeV, and

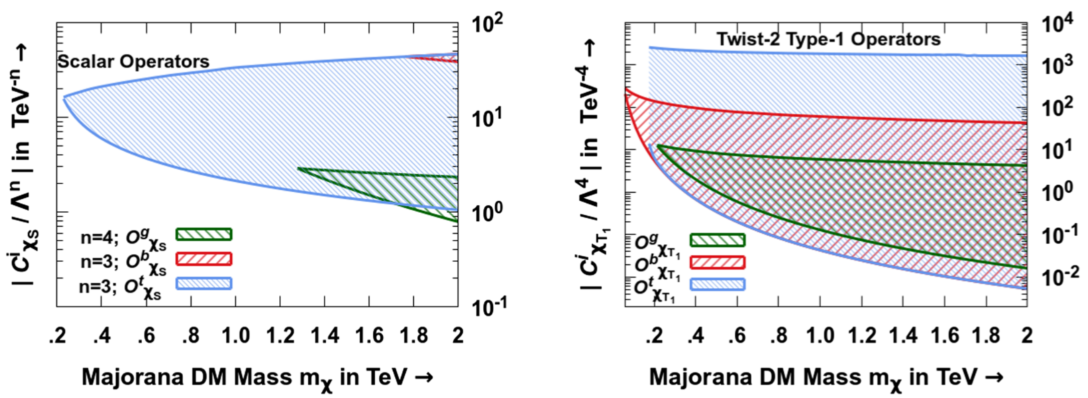

(a) (b)

FIG. 12. The shaded region in Figs. 12(a) and 12(b) depict the allowed range of the Wilson coefficients corresponding to scalar and twist-2 type-2 operators from the relic density constraint [4] and direct detection limits from XENON-1T experiment [6], shown in red, blue, and green for the b-quark, t-quark, and gluonphilic Majorana DM, respectively.

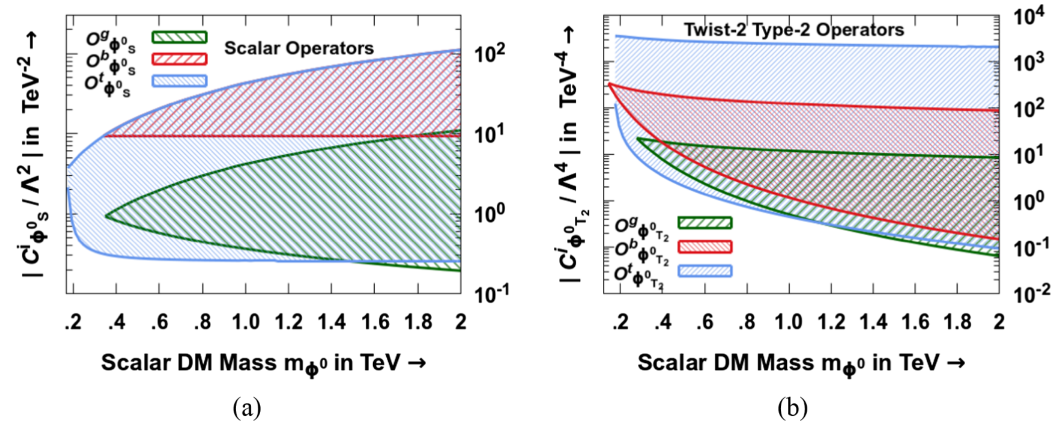

FIG. 13. The shaded region in Figs. 13(a) and 13(b) depict the allowed range of the Wilson coefficients corresponding to scalar and twist-2 type-2 operators from the relic density constraint [4] and direct detection limits from XENON-1T experiment [6], shown in red, blue, and green for the b-quark, t-quark and gluonphilic scalar DM, respectively.

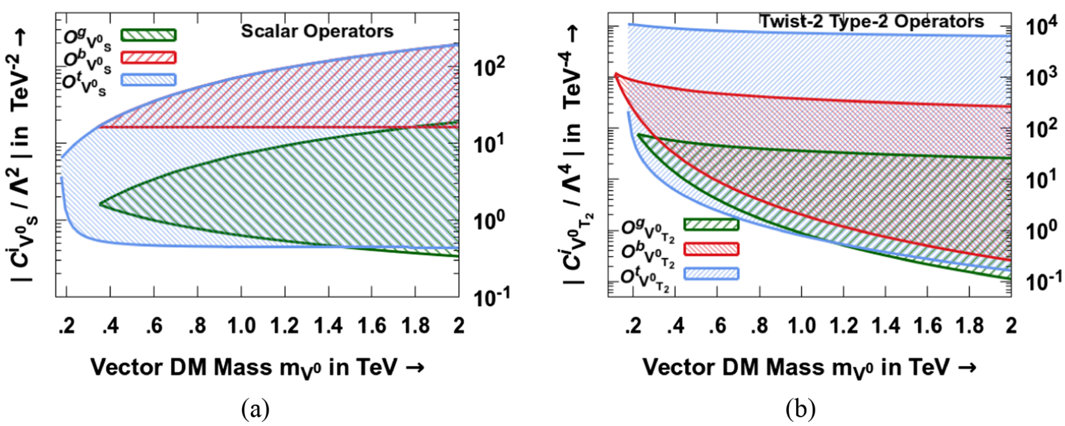

FIG. 14. The shaded region in Figs. 14(a) and 14(b) depict the allowed range of the Wilson coefficients corresponding to scalar and twist-2 type-2 operators from the relic density constraint [4] and direct detection limits from XENON-1T experiment [6], shown in red, blue, and green for the b-quark, t-quark, and gluonphilic vector DM respectively.

350 GeV, respectively. The corresponding contributions induced by twist-2 type-2 DM operators are validated for $m_{V^0} \geq 100$ GeV, 180 GeV, and 200 GeV, respectively as shown in Fig. 14(b).

This analysis shows that the third-generation heavy-quarkphilic and gluonphilic real DM are promising for $m_{\rm DM} \geq 200$ GeV and are likely to be probed and falsified otherwise in the ongoing and future upgraded direct detection experiments. This study also opens up the scope for future collider-based DM search analysis through additional channels induced by the cosmologically constrained operators.

ACKNOWLEDGMENTS

We thank Abhaya Kumar Swain, Debajyoti Choudhury, and Manvinder Pal Singh for fruitful discussions. We acknowledge the partial financial support from core research Grant No. CRG/2018/004889 SERB, Government of India. L. K. S. acknowledges the UGC SRF fellowship for the partial financial support.

APPENDIX A: DM PAIR ANNIHILATION CROSS SECTION

The annihilation cross sections of a pair of Majorana DM χ to a pair of third-generation heavy quarks induced by the scalar, pseudoscalar, axial-vector, and twist-2 type-1 operators are given as

$$\sigma_S(\chi\bar{\chi} \to f\bar{f}) = \mathcal{C}_a \left[\frac{C^f_{\chi S}}{\Lambda^3}\right]^2 \frac{1}{16\pi} m_f^2 \beta_f^3 \beta_\chi\, s, \tag{A1a}$$

$$\sigma_{\rm PS}(\chi\bar{\chi} \to f\bar{f}) = \mathcal{C}_a \left[\frac{C^f_{\chi \rm PS}}{\Lambda^3}\right]^2 \frac{1}{16\pi} m_f^2 \frac{\beta_f}{\beta_\chi}\, s, \tag{A1b}$$

$$\sigma_{\rm AV}(\chi\bar{\chi}\to f\bar{f}) = \mathcal{C}_a\left[\frac{C^f_{\chi_{\rm AV}}}{\Lambda^2}\right]^2\frac{1}{12\pi}[1-4(x_\chi+x_f) + 28x_\chi x_f]\frac{\beta_f}{\beta_\chi}\, s, \tag{A1c}$$

$$\sigma_{T_1}(\chi\bar{\chi}\to f\bar{f}) = \mathcal{C}_a\left[\frac{C^f_{\chi_{T_1}}}{\Lambda^4}\right]^2\frac{1}{960\pi}[4x_\chi^2(92x_f^2+9x_f-8) + 3x_\chi(12x_f^2+9x_f+2) - 32x_f^2+6x_f+8]\frac{\beta_f}{\beta_\chi}\, s^3, \tag{A1d}$$

where $\mathcal{C}_a = 3$, $x_i = m_i^2/s$, and $\beta_i = \sqrt{1-4x_i}$.

As mentioned in the text, we include the study of gluonphilic Majorana DM interactions induced by the scalar, pseudoscalar, and twist-2 type-1 operators. The annihilation cross sections of the Majorana DM pair to a pair of gluons are given as

$$\sigma_S(\chi\bar{\chi}\to gg) = \mathcal{C}_a\mathcal{C}_f\left[\frac{C^g_{\chi_S}}{\Lambda^4}\right]^2\frac{1}{4\pi}\left(\frac{\alpha_s}{\pi}\right)^2 m_\chi^2\beta_\chi\, s^2, \tag{A2a}$$

$$\sigma_{\rm PS}(\chi\bar{\chi}\to gg) = \mathcal{C}_a\mathcal{C}_f\left[\frac{C^g_{\chi_{\rm PS}}}{\Lambda^4}\right]^2\frac{1}{2\pi}\left(\frac{\alpha_s}{\pi}\right)^2 m_\chi^2\beta_\chi\, s^2, \tag{A2b}$$

$$\sigma_{T_1}(\chi\bar{\chi}\to gg) = \mathcal{C}_a\mathcal{C}_f\left[\frac{C^g_{\chi_{T_1}}}{\Lambda^4}\right]^2\frac{1}{80\pi}\left(1+\frac{8}{3}x_\chi\right)\beta_\chi\, s^3, \tag{A2c}$$

where $\mathcal{C}_f = 4/3$.

The annihilation cross sections of a pair of real spin 0 DM ϕ^0 to a pair of third-generation heavy quarks induced by the scalar and twist-2 type-2 operators are given as

$$\sigma_S(\phi^0\phi^0\to f\bar{f}) = \mathcal{C}_a\left[\frac{C^f_{\phi^0_S}}{\Lambda^2}\right]^2\frac{1}{2\pi}m_f^2\frac{\beta_f^3}{\beta_\phi}, \tag{A3a}$$

$$\sigma_{T_2}(\phi^0\phi^0\to f\bar{f}) = \mathcal{C}_a\left[\frac{C^f_{\phi^0_{T_2}}}{\Lambda^4}\right]\frac{1}{240\pi}\frac{\beta_f^3}{\beta_\phi}s^3[2x_\phi^2(23x_f+8) - 4x_\phi(7x_f+2)+6x_f+1]. \tag{A3b}$$

The cross sections for the pair of scalar DM annihilation into a pair of gluons induced by scalar and twist-2 type-2 operators are given as

$$\sigma_S(\phi^0\phi^0\to gg) = \mathcal{C}_a\mathcal{C}_f\left[\frac{C^g_{\phi^0_S}}{\Lambda^2}\right]^2\left(\frac{\alpha_s}{\pi}\right)^2\frac{2}{\pi}\frac{1}{\beta_{\phi^0}}\, s, \tag{A4a}$$

$$\sigma_{T_2}(\phi^0\phi^0\to gg) = \mathcal{C}_a\mathcal{C}_f\left[\frac{C^g_{\phi^0_{T_2}}}{\Lambda^4}\right]^2\frac{1}{60\pi}\beta^3_{\phi^0}\, s^3. \tag{A4b}$$

Similarly, the production of a pair of third-generation heavy quarks as a result of the annihilation of a pair of real vectors DM induced by the scalar, pseudoscalar, axial-vector, and twist-2 type-2 operators is given as

$$\sigma_S(V^0V^0\to f\bar{f}) = \mathcal{C}_a\left[\frac{C^f_{V^0_S}}{\Lambda^2}\right]^2\frac{1}{72\pi}m_f^2\frac{1}{x^2_{V^0}}[1-4x_{V^0} + 12x^2_{V^0}]\frac{\beta_f^3}{\beta_{V^0}}, \tag{A5a}$$

$$\sigma_{\rm PS}(V^0V^0\to f\bar{f}) = \mathcal{C}_a\left[\frac{C^f_{V^0_{\rm PS}}}{\Lambda^4}\right]^2\frac{2}{9\pi}m_f^2\beta_f\beta_{V^0}\, s^2, \tag{A5b}$$

$$\sigma_{\rm AV}(V^0V^0\to f\bar{f}) = \mathcal{C}_a\left[\frac{C^f_{V^0_{\rm AV}}}{\Lambda^2}\right]^2\frac{1}{27\pi}\frac{1}{x_{V^0}}[1-4(x_{V^0}+x_f) + 28x_{V^0}x_f]\beta_f\beta_{V^0}\, s, \tag{A5c}$$

$$\sigma_{T_2}(V^0V^0\to f\bar{f}) = \mathcal{C}_a\left[\frac{C^f_{V^0_{T_2}}}{\Lambda^4}\right]^2\frac{1}{8640\pi}\frac{1}{x^2_{V^0}}[(1+6x_{V^0}) \times(1-4x_{V^0}+12x^2_{V^0})]\beta_f^3\beta^3_{V^0}\, s^3. \tag{A5d}$$

The annihilation cross sections of a pair of vector DM induced by the scalar and twist-2 type-2 gluon currents are given as

$$\sigma_S(V^0V^0\to gg) = \mathcal{C}_a\mathcal{C}_f\left[\frac{C^g_{V^0_S}}{\Lambda^2}\right]^2\frac{1}{18\pi}\left(\frac{\alpha_s}{\pi}\right)^2\frac{1}{x^2_{V^0}} \times[1-4x_{V^0}+12x^2_{V^0}]\frac{1}{\beta_{V^0}}\, s, \tag{A6a}$$

$$\sigma_{\rm PS}(V^0V^0\to gg) = \mathcal{C}_a\mathcal{C}_f\left[\frac{C^g_{V^0_{\rm PS}}}{\Lambda^4}\right]^2\frac{1}{9\pi}\beta_{V^0}\, s^3, \tag{A6b}$$

$$\sigma_{T_2}(V^0V^0\to gg) = \mathcal{C}_a\mathcal{C}_f\left[\frac{C^g_{V^0_{T_2}}}{\Lambda^4}\right]^2\frac{1}{2160\pi}\frac{1}{x^2_{V^0}} \times[1-4x_{V^0}+12x^2_{V^0}]\beta^3_{V^0}\, s. \tag{A6c}$$

APPENDIX B: THERMALLY-AVERAGED ANNIHILATION CROSS SECTION

In order to compute the probability of a DM particle being annihilated by another one, the aforementioned annihilation cross sections are rewritten in terms of the magnitude of relative velocity $|\vec{v}_{\rm DM_1}-\vec{v}_{\rm DM_2}|\equiv|\vec{v}_{\rm DM}|$ and the dimensionless ratio $\xi_f\equiv m_f^2/m_{\rm DM}^2$.

The thermal average of the heavy-quarkphilic Majorana DM pair-annihilation cross sections given in Eqs. (A1a)–(A1d) corresponding to scalar and pseudoscalar operators, respectively are given as

$$\langle\sigma_S(\chi\chi\to f\bar f)|\vec v_\chi|\rangle = \mathcal{C}_a\left[\frac{C^f_{\chi_S}}{\Lambda^3}\right]^2\frac{1}{8\pi}m_f^2 m_\chi^2(1-\xi_f)^{3/2}|\vec v_\chi|^2, \tag{B1a}$$

$$\langle\sigma_{\rm PS}(\chi\chi\to f\bar f)|\vec v_\chi|\rangle = \mathcal{C}_a\left[\frac{C^f_{\chi_{\rm PS}}}{\Lambda^3}\right]^2\frac{1}{8\pi}m_f^2 m_\chi^2(1-\xi_f)^{1/2}\left[4+\frac{1}{2}\frac{\xi_f}{1-\xi_f}|\vec v_\chi|^2\right]. \tag{B1b}$$

The axial-vector contribution is analytically expanded in terms of two independently converging series expansions in terms of $|\vec v_\chi|^2$ and given as

$$\begin{aligned}\langle\sigma_{\rm AV}(\chi\chi\to f\bar f)|\vec v_\chi|\rangle &= \mathcal{C}_a\left[\frac{C^f_{\chi_{\rm AV}}}{\Lambda^2}\right]^2\frac{1}{2\pi}(1-\xi_f)^{1/2}\left[m_\chi^2\left\{\frac{1}{3}\frac{1}{1-\xi_f}|\vec v_\chi|^2+\frac{1}{6}\frac{1}{(1-\xi_f)^2}|\vec v_\chi|^4+\cdots\right\}\right.\\ &\quad\left.+m_f^2\left\{1+\frac{1}{24}\frac{(-28+23\xi_f)}{1-\xi_f}|\vec v_\chi|^2+\frac{(-72-48\xi_f+53\xi_f^2)}{384(1-\xi_f)^2}|\vec v_\chi|^4+\cdots\right\}\right]\\ &= \mathcal{C}_a\left[\frac{C^f_{\chi_{\rm AV}}}{\Lambda^2}\right]^2\frac{1}{2\pi}m_f^2(1-\xi_f)^{1/2}\left[1+\frac{1}{24}\frac{8\xi_f^{-1}-28+23\xi_f}{1-\xi_f}|\vec v_\chi|^2+\cdots\right].\end{aligned} \tag{B1c}$$

And finally the contribution from the twist-2 type-1 operator induced by the heavy quarkphilic Majorana DM interaction is given as

$$\begin{aligned}&\langle\sigma_{T_1}(\chi\chi\to f\bar f)|\vec v_\chi|\rangle\\ &\quad=\mathcal{C}_a\left[\frac{C^f_{\chi_{T_1}}}{\Lambda^4}\right]^2\frac{1}{2\pi}m_\chi^6(1-\xi_f)^{1/2}(2+\xi_f)\\ &\qquad\times\left[1+\frac{1}{48}\frac{56-41\xi-8\xi_f^2+11\xi_f^3}{(1-\xi_f)(2+\xi_f)}|\vec v_\chi|^2\right].\end{aligned} \tag{B1d}$$

Using annihilation cross sections in (A2a)–(A2c) the thermally-averaged annihilation cross sections for the gluonphilic Majorana DM are given as

$$\langle\sigma_S(\chi\chi\to gg)|\vec v_\chi|\rangle=\mathcal{C}_a\mathcal{C}_f\left[\frac{C^g_{\chi_S}}{\Lambda^4}\right]^2\left(\frac{\alpha_s}{\pi}\right)^2\frac{2}{\pi}m_\chi^6|\vec v_\chi|^2, \tag{B2a}$$

$$\langle\sigma_{\rm PS}(\chi\chi\to gg)|\vec v_\chi|\rangle=\mathcal{C}_a\mathcal{C}_f\left[\frac{C^g_{\chi_{\rm PS}}}{\Lambda^4}\right]^2\left(\frac{\alpha_s}{\pi}\right)^2\frac{4}{\pi}m_\chi^6|\vec v_\chi|^2, \tag{B2b}$$

$$\langle\sigma_{T_1}(\chi\chi\to gg)|\vec v_\chi|\rangle=\mathcal{C}_a\mathcal{C}_f\left[\frac{C^g_{\chi_{T_1}}}{\Lambda^4}\right]^2\frac{2}{3\pi}m_\chi^6|\vec v_\chi|^2. \tag{B2c}$$

The thermal average of heavy-quarkphilic scalar DM pair annihilation cross sections displayed in Eqs. (A3a) and (A3b) are given as

$$\begin{aligned}\langle\sigma_S(\phi^0\phi^0\to f\bar f)|\vec v_{\phi^0}|\rangle &= \mathcal{C}_a\left[\frac{C^f_{\phi^0_S}}{\Lambda^2}\right]^2\frac{1}{\pi}m_f^2(1-\xi_f)^{3/2}\\ &\quad\times\left[1-\frac{1}{8}\frac{2-5\xi_f}{1-\xi_f}|\vec v_{\phi^0}|^2\right],\end{aligned} \tag{B3a}$$

$$\begin{aligned}\langle\sigma_{T_2}(\phi^0\phi^0\to f\bar f)|\vec v_{\phi^0}|\rangle &= \mathcal{C}_a\left[\frac{C^f_{\phi^0_{T_2}}}{\Lambda^4}\right]^2\frac{1}{4\pi}m_f^2 m_{\phi^0}^4(1-\xi_f)^{3/2}\\ &\quad\times\left[1+\frac{1}{24}\frac{10-\xi_f}{1-\xi_f}|\vec v_{\phi^0}|^2\right].\end{aligned} \tag{B3b}$$

Similarly, the thermal average of heavy-quarkphilic scalar DM pair annihilation cross sections displayed in Eqs. (A4a) and (A4b) are given as

$$\langle\sigma_S(\phi^0\phi^0\to gg)|\vec v_{\phi^0}|\rangle=\mathcal{C}_a\mathcal{C}_f\left[\frac{C^g_{\phi^0_S}}{\Lambda^2}\right]^2\left(\frac{\alpha_s}{\pi}\right)^2\frac{16}{\pi}m_{\phi^0}^2, \tag{B4a}$$

$$\langle\sigma_{T_2}(\phi^0\phi^0\to gg)|\vec v_{\phi^0}|\rangle = \mathcal{C}_a\mathcal{C}_f\left[\frac{C^g_{\phi^0_{T_2}}}{\Lambda^4}\right]^2\frac{2}{15\pi}m_{\phi^0}^6|\vec v_{\phi^0}|^4. \tag{B4b}$$

The thermal average of the vector DM pair-annihilation cross sections given in Eqs. (A5a)–(A5d) corresponding to the scalar, pseudoscalar, axial-vector, and twist-2 type-2 operators, respectively are given as

$$\begin{aligned}\langle\sigma_S(V^0V^0\to f\bar f)|\vec v_{V^0}|\rangle&=\mathcal{C}_a\left[\frac{C^f_{V^0_S}}{\Lambda^2}\right]^2\frac{1}{3\pi}m_f^2(1-\xi_f)^{3/2}\\ &\quad\times\left[1+\frac{1}{24}\frac{2+7\xi_f}{1-\xi_f}|\vec v_{V^0}|^2\right],\end{aligned} \tag{B5a}$$

$$\langle\sigma_{\rm PS}(V^0V^0\to f\bar f)|\vec v_{V^0}|\rangle = \mathcal{C}_a\left[\frac{C^f_{V^0_{\rm PS}}}{\Lambda^4}\right]^2\frac{16}{9\pi}m_f^2 m_{V^0}^4|\vec v_{V^0}|^2, \tag{B5b}$$

$$\langle\sigma_{\rm AV}(V^0V^0\to f\bar{f})|\vec{v}_{V^0}|\rangle = \mathcal{C}_a\left[\frac{C^f_{V^0_{\rm AV}}}{\Lambda^2}\right]^2\frac{2}{9\pi}m_f^2(1-\xi_f)^{1/2}|\vec{v}_{V^0}|^2, \quad ({\rm B5c})$$

$$\langle\sigma_{T_2}(V^0V^0\to f\bar{f})|\vec{v}_{V^0}|\rangle = \mathcal{C}_a\left[\frac{C^f_{V^0_{T_2}}}{\Lambda^4}\right]^2\frac{1}{90\pi}m^6_{V^0}(1-\xi_f)^{3/2}\times\left[1+\frac{3}{2}\xi_f\right]|\vec{v}_{V^0}|^4. \quad ({\rm B5d})$$

Similarly, the thermal average of the vector DM pair annihilation to gluon channels as displayed in Eqs. (A6a)–(A6c) corresponding to the scalar, pseudoscalar, and twist-2 currents, respectively, are given as

$$\langle\sigma_S(V^0V^0\to gg)|\vec{v}_{V^0}|\rangle = \mathcal{C}_a\mathcal{C}_f\left[\frac{C^g_{V^0_S}}{\Lambda^2}\right]^2\left(\frac{\alpha_s}{\pi}\right)^2\frac{16}{3\pi}m^2_{V^0}\left[1+\frac{1}{3}|\vec{v}_{V^0}|^2\right], \quad ({\rm B6a})$$

$$\langle\sigma_{\rm PS}(V^0V^0\to gg)|\vec{v}_{V^0}|\rangle = \mathcal{C}_a\mathcal{C}_f\left[\frac{C^g_{V^0_{\rm PS}}}{\Lambda^4}\right]^2\left(\frac{\alpha_s}{\pi}\right)^2\frac{64}{9\pi}m^6_{V^0}|\vec{v}_{V^0}|^2, \quad ({\rm B6b})$$

$$\langle\sigma_{T_2}(V^0V^0\to gg)|\vec{v}_{V^0}|\rangle = \mathcal{C}_a\mathcal{C}_f\left[\frac{C^g_{V^0_{T_2}}}{\Lambda^4}\right]^2\frac{2}{45\pi}m^6_{V^0}|\vec{v}_{V^0}|^4. \quad ({\rm B6c})$$

APPENDIX C: EFFECTIVE DM-NUCLEON INTERACTIONS FROM ONE-LOOP DM-GLUON AMPLITUDES

The DM-gluon scattering arising due to the one-loop Feynman-diagrams in Fig. 7 is induced by the scalar, axial-vector, and twist-2 currents of the heavy quarks. We do not consider the contributions of the pseudoscalar operators as they are spin and velocity suppressed. These one-loop amplitudes characterize the effective point interaction Lagrangian for the gluon with Majorana, real scalar and real vector DM candidates, respectively, and are given as

$$\begin{aligned}\mathcal{L}^{\chi\chi gg}_{\rm eff} &= \frac{C^q_{\chi_S}}{\Lambda^3}\frac{\alpha_s}{4\pi}(\bar{\chi}\chi)(G^a)_{\alpha\beta}(G^a)^{\alpha\beta}I^{gg}_S \\ &+ \frac{C^q_{\chi_{\rm AV}}}{\Lambda^2}\frac{\alpha_s}{4\pi}m_\chi(\bar{\chi}i\gamma^5\chi)(\widetilde{G^a})_{\alpha\beta}(G^a)^{\alpha\beta}4I^{gg}_{\rm AV} \\ &+ \frac{C^q_{\chi_{T_1}}}{\Lambda^4}\frac{\alpha_s}{4\pi}\left[\frac{4}{3}\ln\left(\frac{\Lambda^2}{m_Q^2}\right)\right](\bar{\chi}i\partial^\mu\gamma^\nu\chi)\mathcal{O}^g_{\mu\nu}, \end{aligned} \quad ({\rm C1a})$$

$$\begin{aligned}\mathcal{L}^{\phi^0\phi^0 gg}_{\rm eff} &= \frac{C^q_{\phi^0_S}}{\Lambda^2}\frac{\alpha_s}{4\pi}(\phi^0\phi^0)(G^a)_{\alpha\beta}(G^a)^{\alpha\beta}I^{gg}_S \\ &+ \frac{C^q_{\phi^0_{T_2}}}{\Lambda^4}\frac{\alpha_s}{4\pi}\left[\frac{4}{3}\ln\left(\frac{\Lambda^2}{m_Q^2}\right)\right](\phi^0 i\partial^\mu i\partial^\nu\phi^0)\mathcal{O}^g_{\mu\nu}, \end{aligned} \quad ({\rm C1b})$$

$$\begin{aligned}\mathcal{L}^{V^0V^0 gg}_{\rm eff} &= \frac{C^q_{V^0_S}}{\Lambda^2}\frac{\alpha_s}{4\pi}(V^0)^\mu(V^0)_\mu(G^a)^{\alpha\beta}(\widetilde{G^a})_{\alpha\beta}I^{gg}_S \\ &+ \frac{C^q_{V^0_{\rm AV}}}{\Lambda^2}\frac{\alpha_s}{4\pi}(V^0)^{\mu\nu}(\widetilde{V^0})_{\mu\nu}(G^a)^{\alpha\beta}(\widetilde{G^a})_{\alpha\beta}4I^{gg}_{\rm AV} \\ &+ \frac{C^q_{V^0_{T_2}}}{\Lambda^4}\frac{\alpha_s}{4\pi}\left[\frac{4}{3}\ln\left(\frac{\Lambda^2}{m_Q^2}\right)\right](V^0)^\rho i\partial^\mu i\partial^\nu(V^0)_\rho\mathcal{O}^g_{\mu\nu}. \end{aligned} \quad ({\rm C1c})$$

The dimensionless one-loop integrals I^{gg}_S, $I^{gg}_{\rm AV}$, and I^{gg}_T are defined as

$$I^{gg}_S = \int_0^1 dx\int_0^{1-x}dy\frac{1-4xy}{1-\frac{q^2}{m_Q^2}xy}, \quad ({\rm C2a})$$

$$I^{gg}_{\rm AV} = \int_0^1 dx\int_0^{1-x}dy\frac{x^2-x-xy}{1-\frac{q^2}{m_Q^2}xy}, \quad ({\rm C2b})$$

where the square of the four-momentum transferred $q^2\approx 2m_NE_r$ ($E_r\lesssim 100$ KeV is the recoil energy of the nucleon). m_Q and m_N are the concerned heavy quark mass (m_b/m_t) running in the loop and nucleon mass, respectively.

We observe that the one-loop effective contact interactions generated from quark scalar, twist, and axial-vector currents contain the scalar, pseudoscalar, and twist gluon operators, respectively. We perform the nonrelativistic reduction of these operators for zero-momentum partonic gluons and evaluate the gluonic operators between the nucleon states. The zero-momentum gluon contribution to the hadronic matrix element $f^N_{\rm TG}\approx .923$ is extracted in terms of light quarks as [106–108]

$$\begin{aligned}f^N_{TG} &\equiv -\frac{1}{m_N}\langle N|\frac{9}{8}\frac{\alpha_s}{\pi}G^a_{\alpha\beta}G^{\alpha\beta}_a|N\rangle = 1-\sum_{q=u,d,s}f^N_{Tq} \\ &\equiv 1-\sum_{q=u,d,s}\langle N|\frac{m_q}{m_N}(\bar{q}q)|N\rangle. \end{aligned} \quad ({\rm C3})$$

According to [108,109], the pseudoscalar gluon operator between nucleon states is computed as

$$\langle N|G^a_{\alpha\beta}\widetilde{G^{\alpha\beta}_a}|N\rangle = m_N\overline{m}\sum_{q=u,d,s}\frac{1}{m_q}\Delta^{(N)}_q;\ \text{where}$$

$$\bar{m} = \left[\frac{1}{m_u}+\frac{1}{m_d}+\frac{1}{m_s}\right]^{-1}. \quad ({\rm C4})$$

The axial-vector current $\langle N|\bar{q}\gamma^\mu\gamma^5 q|N\rangle = 2\Delta_q^{(N)} s^\mu$ specifies the coefficient $\Delta_q^{(N)}$ as the spin content of the nucleon's quark q. The coefficients for light quarks satisfy $\Delta_u^{(p)} = \Delta_d^{(n)}$, $\Delta_u^{(n)} = \Delta_d^{(p)}$ and $\Delta_s^{(p)} = \Delta_s^{(n)}$, while the contribution from heavy quarks is found to be vanishingly small [110]. It is important to observe that a quark axial-vector current is related to the gluonic pseudoscalar current by PCAC [109]. The zero-momentum nucleonic matrix element for gluon twist-2 operators is defined as

$$\langle N|\mathcal{O}^g_{\mu\nu}|N\rangle = -\frac{1}{m_N}\left[k^\mu k^\nu - \frac{1}{4}g^{\mu\nu}m_N^2\right]g(2;\mu_\mathrm{R}),$$

$$\text{where } g(2;\mu_\mathrm{R}) = \int_0^1 x g(x;\mu_\mathrm{R})dx. \tag{C5}$$

[1] Vera C. Rubin and W. Kent Ford, Jr., Astrophys. J. **159**, 379 (1970).
[2] D. Clowe, M. Bradac, A. H. Gonzalez, M. Markevitch, S. W. Randall, C. Jones, and D. Zaritsky, Astrophys. J. Lett. **648**, L109 (2006).
[3] E. Komatsu *et al.* (WMAP Science Team), Prog. Theor. Exp. Phys. **2014**, 06B102 (2014).
[4] N. Aghanim *et al.* (Planck Collaboration), Astron. Astrophys. **641**, A6 (2020).
[5] D. S. Akerib *et al.* (LUX Collaboration), Nucl. Instrum. Methods Phys. Res., Sect. A **704**, 111 (2013).
[6] E. Aprile *et al.* (XENON Collaboration), Phys. Rev. Lett. **121**, 111302 (2018).
[7] P. Agnes *et al.* (DarkSide Collaboration), Phys. Rev. Lett. **121**, 081307 (2018).
[8] Y. Meng *et al.* (PandaX-4T Collaboration), Phys. Rev. Lett. **127**, 261802 (2021).
[9] A. H. Abdelhameed *et al.* (CRESST Collaboration), Phys. Rev. D **100**, 102002 (2019).
[10] C. Amole *et al.* (PICO Collaboration), Phys. Rev. D **100**, 022001 (2019).
[11] E. Behnke, M. Besnier, P. Bhattacharjee, X. Dai, M. Das, A. Davour, F. Debris, N. Dhungana, J. Farine, M. Fines-Neuschild *et al.*, Astropart. Phys. **90**, 85 (2017).
[12] M. Schumann, J. Phys. G **46**, 103003 (2019).
[13] M. Bauer and T. Plehn, Lect. Notes Phys. **959**, 86 (2019).
[14] J. Billard, M. Boulay, S. Cebrián, L. Covi, G. Fiorillo, A. Green, J. Kopp, B. Majorovits, K. Palladino, F. Petricca *et al.*, Rep. Prog. Phys. **85**, 056201 (2022).
[15] M. Ackermann *et al.* (Fermi-LAT Collaboration), Phys. Rev. Lett. **115**, 231301 (2015).
[16] V. A. Acciari *et al.* (MAGIC Collaboration), Phys. Dark Universe **28**, 100529 (2020).
[17] H. Abdallah *et al.* (H.E.S.S. Collaboration), Phys. Rev. Lett. **117**, 111301 (2016).
[18] R. Abbasi *et al.* (IceCube Collaboration), Proc. Sci., ICRC2019 (**2020**) 541.
[19] A. Albert *et al.* (ANTARES Collaboration), Phys. Lett. B **805**, 135439 (2020).
[20] K. Bays *et al.* (Super-Kamiokande Collaboration), Phys. Rev. D **85**, 052007 (2012).
[21] N. F. Bell, G. Busoni, and I. W. Sanderson, J. Cosmol. Astropart. Phys. 03 (2017) 015.
[22] A. Albert, M. Bauer, J. Brooke, O. Buchmueller, D. G. Cerdeño, M. Citron, G. Davies, A. De Cosa, A. De Roeck, A. De Simone *et al.*, Phys. Dark Universe **16**, 49 (2017).
[23] P. Ko, A. Natale, M. Park, and H. Yokoya, J. High Energy Phys. 01 (2017) 086.
[24] C. Englert, M. McCullough, and M. Spannowsky, Phys. Dark Universe **14**, 48 (2016).
[25] T. Abe *et al.* (LHC Dark Matter Working Group), Phys. Dark Universe **27**, 100351 (2020).
[26] S. Dutta, A. Goyal, and L. K. Saini, J. High Energy Phys. 02 (2018) 023.
[27] M. Bauer, M. Klassen, and V. Tenorth, J. High Energy Phys. 07 (2018) 107.
[28] M. Bauer, U. Haisch, and F. Kahlhoefer, J. High Energy Phys. 05 (2017) 138.
[29] S. Baek, P. Ko, and J. Li, Phys. Rev. D **95**, 075011 (2017).
[30] A. Carrillo-Monteverde, Y. J. Kang, H. M. Lee, M. Park, and V. Sanz, J. High Energy Phys. 06 (2018) 037.
[31] S. Kraml, U. Laa, K. Mawatari, and K. Yamashita, Eur. Phys. J. C **77**, 326 (2017).
[32] G. Aad *et al.* (ATLAS Collaboration), Eur. Phys. J. C **82**, 105 (2022).
[33] R. C. Cotta, J. L. Hewett, M. P. Le, and T. G. Rizzo, Phys. Rev. D **88**, 116009 (2013).
[34] J. Y. Chen, E. W. Kolb, and L. T. Wang, Phys. Dark Universe **2**, 200 (2013).
[35] A. Crivellin, U. Haisch, and A. Hibbs, Phys. Rev. D **91**, 074028 (2015).
[36] P. Athron *et al.* (GAMBIT Collaboration), Eur. Phys. J. C **81**, 992 (2021).
[37] I. Bischer, T. Plehn, and W. Rodejohann, SciPost Phys. **10**, 039 (2021).
[38] B. Barman, S. Bhattacharya, S. Girmohanta, and S. Jahedi, J. High Energy Phys. 04 (2022) 146.
[39] H. Bharadwaj and S. Dutta, arXiv:1901.00192.
[40] H. Bharadwaj and A. Goyal, Chin. Phys. C **45**, 023114 (2021).
[41] N. Chen, J. Wang, and X. P. Wang, arXiv:1501.04486.
[42] H. Dreiner, M. Huck, M. Krämer, D. Schmeier, and J. Tattersall, Phys. Rev. D **87**, 075015 (2013).
[43] Y. J. Chae and M. Perelstein, J. High Energy Phys. 05 (2013) 138.
[44] P. J. Fox, R. Harnik, J. Kopp, and Y. Tsai, Phys. Rev. D **85**, 056011 (2012).
[45] N. F. Bell, J. B. Dent, A. J. Galea, T. D. Jacques, L. M. Krauss, and T. J. Weiler, Phys. Rev. D **86**, 096011 (2012).

[46] S. Dutta, D. Sachdeva, and B. Rawat, Eur. Phys. J. C **77**, 639 (2017).
[47] F. Kahlhoefer, Int. J. Mod. Phys. A **32**, 1730006 (2017).
[48] V. A. Mitsou, J. Phys. Conf. Ser. **651**, 012023 (2015).
[49] A. Boveia and C. Doglioni, Annu. Rev. Nucl. Part. Sci. **68**, 429 (2018).
[50] A. De Simone and T. Jacques, Eur. Phys. J. C **76**, 367 (2016).
[51] B. Bhattacherjee, D. Choudhury, K. Harigaya, S. Matsumoto, and M. M. Nojiri, J. High Energy Phys. 04 (2013) 031.
[52] S. Baek, P. Ko, and P. Wu, J. Cosmol. Astropart. Phys. 07 (2018) 008.
[53] C. Kilic, M. D. Klimek, and J. H. Yu, Phys. Rev. D **91**, 054036 (2015).
[54] M. A. Gomez, C. B. Jackson, and G. Shaughnessy, J. Cosmol. Astropart. Phys. 12 (**2014**) 025.
[55] B. Fuks, J. Phys. Conf. Ser. **1271**, 012017 (2019).
[56] S. Colucci, B. Fuks, F. Giacchino, L. Lopez Honorez, M. H. G. Tytgat, and J. Vandecasteele, Phys. Rev. D **98**, 035002 (2018).
[57] M. Garny, J. Heisig, M. Hufnagel, and B. Lülf, Phys. Rev. D **97**, 075002 (2018).
[58] Y. Zhang, Phys. Lett. B **720**, 137 (2013).
[59] A. M. Sirunyan *et al.* (CMS Collaboration), J. High Energy Phys. 03 (2019) 141.
[60] A. M. Sirunyan *et al.* (CMS Collaboration), Phys. Rev. Lett. **122**, 011803 (2019).
[61] G. Aad *et al.* (ATLAS Collaboration), Eur. Phys. J. C **81**, 860 (2021).
[62] CMS Collaboration, Report No. CMS-PAS-B2G-15-007, CERN, https://cds.cern.ch/record/2138506?ln=en.
[63] T. Lin, E. W. Kolb, and L. T. Wang, Phys. Rev. D **88**, 063510 (2013).
[64] U. Haisch, F. Kahlhoefer, and J. Unwin, J. High Energy Phys. 07 (2013) 125.
[65] J. Goodman, M. Ibe, A. Rajaraman, W. Shepherd, T. M. P. Tait, and H. B. Yu, Phys. Rev. D **82**, 116010 (2010).
[66] C. Arina, M. Backović, E. Conte, B. Fuks, J. Guo, J. Heisig, B. Hespel, M. Krämer, F. Maltoni, A. Martini *et al.*, J. High Energy Phys. 11 (2016) 111.
[67] O. Mattelaer and E. Vryonidou, Eur. Phys. J. C **75**, 436 (2015).
[68] Manuel Drees and Mihoko M. Nojiri, Phys. Rev. D **48**, 3483 (1993).
[69] J. Hisano, K. Ishiwata, and N. Nagata, Phys. Rev. D **82**, 115007 (2010).
[70] J. Hisano, K. Ishiwata, N. Nagata, and M. Yamanaka, Prog. Theor. Phys. **126**, 435 (2011).
[71] J. Hisano, K. Ishiwata, N. Nagata, and T. Takesako, J. High Energy Phys. 07 (2011) 005.
[72] J. Hisano, K. Ishiwata, and N. Nagata, Phys. Lett. B **706**, 208 (2011).
[73] J. Hisano, K. Ishiwata, and N. Nagata, Phys. Rev. D **87**, 035020 (2013).
[74] J. Hisano, R. Nagai, and N. Nagata, J. High Energy Phys. 05 (2015) 037.
[75] J. Hisano, K. Ishiwata, and N. Nagata, J. High Energy Phys. 06 (2015) 097.
[76] A. Carrillo-Monteverde, Y. J. Kang, H. M. Lee, M. Park, and V. Sanz, Proc. Sci., ICHEP2018 (**2019**) 351.
[77] E. Morgante, Adv. High Energy Phys. **2018**, 5012043 (2018).
[78] H. M. Lee, M. Park, and V. Sanz, J. High Energy Phys. 05 (2014) 063.
[79] P. Gondolo and G. Gelmini, Nucl. Phys. **B360**, 145 (1991).
[80] E. W. Kolb and M. S. Turner, Front. Phys. **69**, 1 (1990).
[81] M. Backovic, K. Kong, and M. McCaskey, Phys. Dark Universe **5–6**, 18 (2014).
[82] F. Ambrogi, C. Arina, M. Backovic, J. Heisig, F. Maltoni, L. Mantani, O. Mattelaer, and G. Mohlabeng, Phys. Dark Universe **24**, 100249 (2019).
[83] N. D. Christensen and C. Duhr, Comput. Phys. Commun. **180**, 1614 (2009).
[84] A. Alloul, N. D. Christensen, C. Degrande, C. Duhr, and B. Fuks, Comput. Phys. Commun. **185**, 2250 (2014).
[85] G. Belanger, F. Boudjema, A. Pukhov, and A. Semenov, Nuovo Cimento C **033N2**, 111 (2010).
[86] J. Kumar and D. Marfatia, Phys. Rev. D **88**, 014035 (2013).
[87] M. Ackermann *et al.* (Fermi-LAT Collaboration), Phys. Rev. D **91**, 122002 (2015).
[88] M. Aguilar *et al.* (AMS Collaboration), Phys. Rev. Lett. **113**, 121102 (2014).
[89] M. Aguilar *et al.* (AMS Collaboration), Phys. Rev. Lett. **117**, 091103 (2016).
[90] A. Abramowski *et al.* (H.E.S.S. Collaboration), Phys. Rev. Lett. **106**, 161301 (2011).
[91] A. Abramowski *et al.* (H.E.S.S. Collaboration), Phys. Rev. Lett. **110**, 041301 (2013).
[92] H. Abdallah *et al.* (H.E.S.S. Collaboration), Phys. Rev. D **102**, 062001 (2020).
[93] H. León Vargas, A. Sandoval, E. Belmont, and R. Alfaro, Adv. Astron. **2017**, 1932413 (2017).
[94] A. Albert *et al.* (HAWC Collaboration), Astrophys. J. **853**, 154 (2018).
[95] J. Lundeen (HAWC Collaboration), Proc. Sci., ICRC2019 (**2021**) 529.
[96] T. Sjöstrand, S. Ask, J. R. Christiansen, R. Corke, N. Desai, P. Ilten, S. Mrenna, S. Prestel, C. O. Rasmussen, and P. Z. Skands, Comput. Phys. Commun. **191**, 159 (2015).
[97] J. M. Zheng, Z. H. Yu, J. W. Shao, X. J. Bi, Z. Li, and H. H. Zhang, Nucl. Phys. **B854**, 350 (2012).
[98] Z. H. Yu, J. M. Zheng, X. J. Bi, Z. Li, D. X. Yao, and H. H. Zhang, Nucl. Phys. **B860**, 115 (2012).
[99] J. Pumplin, D. R. Stump, J. Huston, H. L. Lai, P. M. Nadolsky, and W. K. Tung, J. High Energy Phys. 07 (2002) 012.
[100] A. Buckley, J. Ferrando, S. Lloyd, K. Nordström, B. Page, M. Rüfenacht, M. Schönherr, and G. Watt, Eur. Phys. J. C **75**, 132 (2015).
[101] A. Belyaev, E. Bertuzzo, C. Caniu Barros, O. Eboli, G. Grilli Di Cortona, F. Iocco, and A. Pukhov, Phys. Rev. D **99**, 015006 (2019).
[102] S. Kang, S. Scopel, G. Tomar, and J. H. Yoon, Astropart. Phys. **114**, 80 (2020).

[103] S. Kang, S. Scopel, G. Tomar, and J. H. Yoon, Astropart. Phys. **109**, 50 (2019).
[104] R. H. Helm, Phys. Rev. **104**, 1466 (1956).
[105] J. D. Lewin and P. F. Smith, Astropart. Phys. **6**, 87 (1996).
[106] M. Cirelli, E. Del Nobile, and P. Panci, J. Cosmol. Astropart. Phys. 10 (2013) 019.
[107] G. Belanger, F. Boudjema, A. Pukhov, and A. Semenov, Comput. Phys. Commun. **185**, 960 (2014).
[108] H. Y. Cheng and C. W. Chiang, J. High Energy Phys. 07 (2012) 009.
[109] H. Y. Cheng, Phys. Lett. B **219**, 347 (1989).
[110] M. V. Polyakov, A. Schafer, and O. V. Teryaev, Phys. Rev. D **60**, 051502 (1999).